Volume 16
Number 4
28 January 2024
Pages 1431-2062

Nanoscale

rsc.li/nanoscale

ISSN 2040-3372

ROYAL SOCIETY OF CHEMISTRY

REVIEW ARTICLE
Thalappil Pradeep *et al.*
A concise guide to chemical reactions of atomically precise noble metal nanoclusters

NCNST

Nanoscale

ROYAL SOCIETY OF CHEMISTRY

REVIEW

View Article Online
View Journal | View Issue

Cite this: *Nanoscale*, 2024, **16**, 1446

A concise guide to chemical reactions of atomically precise noble metal nanoclusters

Paulami Bose, Krishnadas Kumaranchira Ramankutty,† Papri Chakraborty, ‡ Esma Khatun and Thalappil Pradeep *

Received 11th October 2023,
Accepted 11th November 2023

DOI: 10.1039/d3nr05128e

rsc.li/nanoscale

Nanoparticles (NPs) with atomic precision, known as nanoclusters (NCs), are an emerging field in materials science in view of their fascinating structure–property relationships. Ultrasmall noble metal NPs have molecule-like properties that make them fundamentally unique compared with their plasmonic counterparts and bulk materials. In this review, we present a comprehensive account of the chemistry of monolayer-protected atomically precise noble metal nanoclusters with a focus on the chemical reactions, their diversity, associated kinetics, and implications. To begin with, we briefly review the history of the evolution of such precision materials. Then the review explores the diverse chemistry of noble metal nanoclusters, including ligand exchange reactions, ligand-induced structural transformations, and reactions with metal ions, metal thiolates, and halocarbons. Just as molecules do, these precision materials also undergo intercluster reactions in solution. Supramolecular forces between these systems facilitate the creation of well-defined hierarchical assemblies, composites, and hybrid materials. We conclude the review with a future perspective and scope of such chemistry.

1. Introduction

Richard Feynman's historic Caltech address, *There's Plenty of Room at the Bottom*, in 1959, discussed the concept of nanotechnology which envisioned "maneuvering things atom by atom".[1] Development of atomically precise metal nanoclusters may be viewed as a direction to create materials atom by atom. The term 'metal cluster' was originally defined by Cotton in 1964 as "*a finite group of metal atoms which are held together mainly or at least to a significant extent, by bonds directly between the metal atoms, even though some nonmetal atoms may also be intimately associated with the cluster*" to refer to coordination compounds.[2,3] This term was also used in the early literature to refer to plasmonic noble metal particles consisting of several hundreds or a few thousands of atoms, although the term 'metal nanocluster' is nowadays used more appropriately to refer to atomically precise, bare, or ligand-protected particles with a precise, molecule-like composition (M_xL_y; M = metal atom, L = ligands such as thiolate, phosphine, *etc.*) and well-defined properties. Precision refers to structure as well, both in the molecular form in the gaseous, solution and solid states. Therefore, clusters in the context of this review may be defined as "*a finite group of atoms with precise composition and structure, composed of two or more metal atoms held together by chemical bonds between them, and the structure formed stands protected or unprotected with ligands, with well-defined properties.*"

Electronic confinement of noble metals has been an important subject matter of research in the past few decades.[4–6] As the particle size shrinks below ~3 nm to an intermediate size regime, bridging the dimensions of molecules and condensed matter, molecule-like properties arise in such materials.[4,7] Such molecular materials are called atomically precise noble metal nanoclusters (NCs), which have precise composition, structure, and unique properties.[7–11] $Au_{102}(p\text{-MBA})_{44}$ nanocluster (*p*-MBA=*para*-mercaptobenzoic acid) was the first reported single-crystal structure in the family of thiolate-protected atomically precise nanoclusters,[12] although clusters such as $Au_{11}I_3[P(C_6H_4\text{-}p\text{-}Cl)_3]_7$ (ref. 13) and $[Au_{13}(PPhMe_2)_{10}C_{12}]^{3+}$ (ref. 14) were known since 1970, with other ligands. Since then, more than 250 nanocluster crystal structures have been published.[7,11,15] Many more noble metal nanoclusters with proteins,[16–21] DNA,[22–27] poly(amidoamine)-based dendrimers,[28–31] and cyclodextrins[32–34] are now known.[11] Today, atomic precision in assemblies is attainable in several materials, such as metals, metal oxides, semi-

DST Unit of Nanoscience & Thematic Unit of Excellence, HSB 148, Indian Institute of Technology Madras, Chennai-600036, Tamil Nadu, India.
E-mail: pradeep@iitm.ac.in
†Present address: School of Chemistry, Indian Institute of Science Education and Research Thiruvananthapuram, Vithura, Thiruvananthapuram-695551, Kerala, India.
‡Present address: Institute of Nanotechnology, Karlsruhe Institute of Technology, 76344 Eggenstein-Leopoldshafen, and Institute of Physical Chemistry, Karlsruhe Institute of Technology, 76131 Karlsruhe, Germany.

conductors, ionic compounds, and even rare gases.[35] Carbon clusters, such as Buckminsterfullerene or C_{60}, are some of the most popular clusters investigated so far.[36,37] Molecular clusters such as $(H_2O)_{2,3,4...}$ and $(CH_3OH)_n(H_2O)_m$, where n, m = 1,2,3,..., and zero-dimensional (0D) particles of perovskites, graphene, *etc.*, are also gaining interest.[38,39] In our latest book we presented a comprehensive overview of noble metal nanoclusters and their properties, with a compendium of all reported clusters.[15] However, in this review, we will be focusing on the thiolate and phosphine-protected nanoclusters in the context of their chemical reactions.

Noble metal nanoclusters exhibit well-defined physical, chemical, and electronic properties.[7,11,12] Unique characteristic properties of nanoclusters include discrete electronic structures,[40–47] corresponding HOMO–LUMO transitions,[48–53] chemical reactivity,[10,54–56,57–59] photoluminescence[60–63] and intrinsic magnetism.[64–69] Metal nanoclusters have attracted tremendous interest from the scientific community due to their potential applications in optoelectronics,[70,71] sensing,[63,72–74,75] bioimaging,[63,76–79,80] catalysis,[8,81–83,84] and others.[7,11]

Today, the chemistry of well-defined monolayer-protected nanoclusters is an active area of research. We present this review as a mini guide to ligand-protected atomically precise metal nanoclusters and their diverse chemistry (schematically represented in Fig. 1). To begin with, we trace the origin and landmark developments in nanocluster science. The article presents the recent research on ligand-induced chemistry, intercluster & interparticle reactions and their mechanism, thermodynamics, kinetics, and implications. Knowledge of the precise chemical reactivity of such nanoclusters gives a way to control their composition to form alloys and hybrid materials, and also for engineering their properties. Such new materials may find suitable roles in photophysical, catalytic, and optoelectronic applications. Chemical reactions between nanomaterials of various types provide new insights into the dynamics at the nanoscale. Reactivity at the nanoscale is of importance to chemistry in general, and to catalysis, functional materials, photophysics, nanomedicines, sensors, and clean water, in particular.

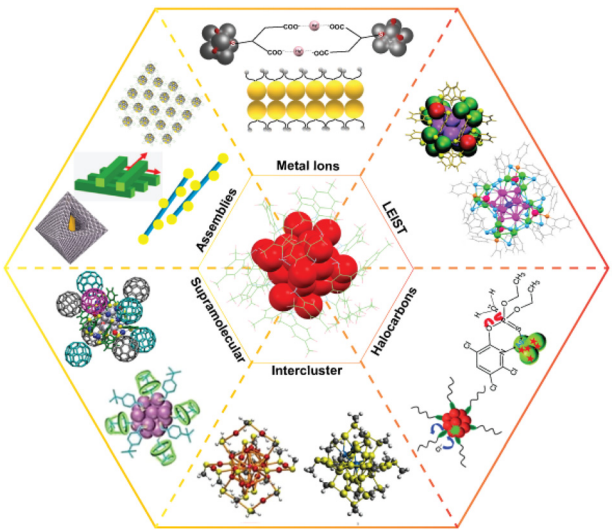

Fig. 1 Schematic illustration of the diverse chemistry of the ligand-protected atomically precise noble metal nanoclusters. Images under assemblies are adapted with permission from ref. 275, 281, 278 and 285. Copyright 2014 and 2018 John Wiley and Sons. Copyright 2014 American Chemical Society. Copyright 2020 The Royal Society of Chemistry. Images under halocarbons are adapted from ref. 258 and 257. Copyright 2013 Royal Society of Chemistry. Images under supramolecular are adapted from ref. 259 and 260. Copyright 2014 and 2018 American Chemical Society. Images under intercluster are adapted from ref. 55. Copyright 2016 Springer Nature Group. Images under LEIST are adapted from ref. 218 and 176. Copyright 2018 Royal Society of Chemistry. Copyright 2020 American Chemical Society.

2. Atomically precise noble metal nanoclusters: the evolution

Size-dependent studies of colloidal silver particles in solution using radiolytic and electrochemical methods by Henglein *et al.* in the 1980s were among the earliest experiments using nanoscale noble metals.[85–88] Haruta's discovery, in 1989, of the catalytic activity of finely divided, nanosized gold particles supported on oxide surfaces boosted research on noble metal NPs.[89] However, most of the early insights into atomically precise metal nanoclusters were derived from gas-phase investigations.

2.1. Insights from gas-phase studies

Gas-phase studies provided the first glimpses into the characteristics of metal nanoclusters. Nanoclusters of alkali, alkaline earth, and noble metals have been studied extensively since the 1980s. Gas-phase investigations of metal nanoclusters made extensive use of techniques like mass spectrometry, ion mobility spectrometry, photoelectron spectroscopy, vibrational spectroscopy, *etc.*[90,91] Using mass spectrometry, Knight *et al.* characterized sodium Na_n (n = 4–100) metal nanoclusters in the gas phase.[92] The most abundant peaks observed correspond to the nanoclusters with n = 8, 20, 40, 58, and 92. According to the jellium model, the electrons in these nanoclusters are distributed into discrete electronic shells, just as in atoms. The numbers 8, 20, 40, 58, and 92 correspond to the total number of valence electrons ($3s^1$) in these nanoclusters, analogous to the valence shell electron configurations of noble gases. The nanoclusters whose valence shell electron counts fall in this series of 'magic' numbers are referred to as 'magic clusters'. The abundance of these nanoclusters in the mass spectra is attributed to their stability gained from the completion of electronic shell structures, just like noble gases. This is one of the reasons for the fact that 'every atom counts' in the case of atomically precise metal nanoclusters. Magic nanoclusters of metals such as aluminum were also observed. For example, Khanna *et al.*, showed that Al_{13}^-, which has a magic number of 40 electrons, exhibits special inertness towards gas-phase etching reactions.[93,94] Such nanoclusters are also called 'superatoms', a term coined by Khanna *et al.* in 1995.[95] They also introduced the idea of using superatomic nanoclusters as building blocks for nanocluster-assembled

materials. The stability of gas-phase metal nanoclusters, especially larger ones, depends on closed geometric shells as well as electronic shells. In the gas phase, the geometry of the nanocluster, rather than the electronic structure, determines the stability. Due to the overlap of electronic bands, there is a negligible change in electronic energy with the addition of each new atom to the nanocluster. For example, positively charged calcium nanoclusters in the gas phase such as Ca_{561}, Ca_{1412}, Ca_{2865}, *etc.*, exhibit mass spectral abundance which is ascribed to the successive addition of layers of atoms to form stable geometries.[96] Bare gold nanoclusters in the gas phase have been investigated since the 1980s. Kappes *et al.* used ion mobility (IM) measurements and trapped ion electron diffraction[97–99] in conjunction with density functional theory (DFT) calculations in order to assign structures of Au_n^- (n < 13) nanoclusters[98] and also suggested that planar to three-dimensional transition in these nanoclusters occurs at n = 11.[98] The structure of unprotected noble metal nanoclusters deposited on surfaces has also been probed using techniques such as scanning tunneling microscopy.[100,101]

2.2. Atomically precise metal nanoclusters in solution: phosphine- and thiolate-protected metal nanoclusters

Solution-phase nanochemistry of noble metals was accelerated after the discovery of the Brust–Schiffrin method reported in 1994,[102] wherein thiolates were used as protecting ligands with limited information on the structure and composition of these particles.

The earliest examples of atomically precise metal cluster compounds studied in the solution phase were gold–phosphine coordination complexes, like $Au_{11}(PPh_3)_7(SCN)_3$ and $Au_{11}I_3(P(C_6H_4\text{-}p\text{-}Cl)_3)_7$. These compounds were synthesized in 1969 and 1970, respectively.[13,103] $Au_{11}X_3[PR_3]_7$ is the first known crystal structure with an incomplete icosahedral core.[13] In 1981, Briant *et al.* reported the first$[Au_{13}(PPhMe_2)_{10}C_{12}]^{3+}$ nanocluster consisting of a perfect icosahedral core.[14] Bigger nanoclusters such as $[Au_{39}(PPh_3)_{14}Cl_6]Cl_2$ consisting of larger, atomically precise Au cores were reported in 1992.[104] Schmid *et al.* synthesized the well-known molecule, $Au_{55}[P(C_6H_5)_3]_{12}CI_6$, in 1981, which attracted significant attention in the community.[105] The crystal structure of this nanocluster remained elusive; however, insights into its structure came from later studies.[106] Though techniques such as fast atom bombardment mass spectrometry (FABMS) were used to analyze compounds such as $[Pt_2(AuPPh_3)_{10}Ag_{13}Cl_7]$, *etc.*,[107] single-crystal X-ray diffraction was the major tool for probing their compositions and structures. Extensive reviews are available on the single-crystal structure of atomically precise nanoclusters.[7,11,108]

Even though phosphine-protected noble metal nanoclusters have been known since the 1960s as mentioned above, the big leap in the field of solution-phase nanochemistry of noble metals occurred only after the pioneering efforts of the Whetten and Murray research groups on thiolate-protected noble metal particles. In 1996, Whetten *et al.* were the first to observe atomically precise compositions for thiolate-protected gold particles using mass spectrometry. Particles with such compositions were referred to as 'nanocrystal gold molecules'.[109] Murray *et al.* electrochemically observed a molecule-like electronic structure for many such particles. In 2005, Shichibu *et al.* synthesized glutathione (SG)-protected $Au_{25}(SG)_{18}$ nanocluster *via* ligand exchange reaction of pre-formed Au-phosphine nanoclusters.[110–112] In the same year, Tsukuda *et al.* mass spectrometrically observed a series of glutathione-protected gold nanoclusters with precise and molecule-like compositions, such as $Au_{10}(SG)_{10}$, $Au_{15}(SG)_{13}$, $Au_{18}(SG)_{14}$, $Au_{22}(SG)_{16}$, $Au_{22}(SG)_{17}$, $Au_{25}(SG)_{18}$, $Au_{29}(SG)_{20}$, $Au_{33}(SG)_{22}$, and $Au_{39}(SG)_{24}$ which were separated by polyacrylamide gel electrophoresis (PAGE).[113] In 2006, Häkkinen *et al.* proposed the 'divide and protect' structural model wherein these nanoclusters were viewed as consisting of a discrete metal core, protected by well-defined metal–ligand oligomeric units.[114] In 2007, Whetten *et al.* unambiguously assigned the composition of the most popular nanocluster in this family, $Au_{25}(PET)_{18}$ (PET = 2-phenylethanethiolate) (which was wrongly assigned as $Au_{38}(PET)_{24}$ in earlier investigations) through electrospray ionization mass spectrometry (ESI MS). In 2007, Shichibu *et al.* synthesized a biicosahderal nanocluster, $[Au_{25}(PPh_3)_{10}(SC_nH_{2n+1})_5Cl_2]^{2+}$ (n = 2–18) by the chemical reaction between $[Au_{11}(PPh_3)_8Cl_2]^+$ and n-alkanethiol ($C_nH_{2n+1}SH$, n = 2, 8, 10, 12, 14, 16, and 18).[115] This was the first Au_{25} nanocluster compound whose crystal structure was resolved. Apart from thiolate and phosphinate monolayers, anion templates, such as halides,[116] sulfides,[117] chalcogenides,[118] and polyoxometalates,[119,120] are becoming increasingly prominent in the preparation of high-nuclearity atomically precise Ag nanoclusters.[121] Mass spectrometry, separation techniques such as electrophoresis, size-exclusion chromatography (SEC), and single-crystal X-ray diffraction have made tremendous contributions to the science of ligand-protected noble metal nanoclusters.[91,122,123] Recently, microelectron diffraction has been used to resolve the structures of those nanoclusters for which crystallization was difficult.[124,125] Computational methods have made significant contributions to our understanding of the structures and properties of these nanoclusters, complementing the experimental approaches.[9,41,47,50,126–129]

2.3. Early insights into structures

The identification of atomically precise nanoclusters such as $Au_{25}(PET)_{18}$ sparked extensive research into numerous nanoclusters and their properties; however, the structures of these early nanoclusters remained unknown for quite some time. Therefore, these particles were called 'monolayer-protected nanoclusters' (MPCs); the term was originally used to refer to their larger (consisting of a few hundred metal atoms), plasmonic counterparts wherein the protecting ligands were assumed to be arranged in a uniform, 2D fashion, as in the case of self-assembled monolayers (SAMs)[130] of ligands on metals. In 2007, Kornberg *et al.* were the first to resolve the crystal structure of a thiolate-protected gold nanocluster, namely $Au_{102}(MBA)_{44}$ (MBA = p-mercaptobenzoic acid).[131]

$Au_{102}(MBA)_{44}$ provided significant new insights into the structure of the ligands on the NPs. $Au_{102}(MBA)_{44}$ consists of an Au_{79} core protected by nineteen $Au(SR)_2$ and two $Au_2(SR)_3$ units, often referred to as staple units. In 2008, the crystal structure of $Au_{25}(SR)_{18}$, one of the most popular members of this family of nanoclusters,[132] was resolved independently by Akola *et al.* and Heaven *et al.*, which showed that it consisted of an Au_{13} icosahedron protected by six $Au_2(SR)_3$ oligomeric staples.[133,134] These findings proved that the structural arrangement of protecting ligands on metal NPs can be completely different from that of SAMs. Recently, atomic precision has been achieved in a larger size regime of nanoclusters wherein plasmonic features start appearing. For example, structures of $Au_{279}(SPh\text{-}tBu)_{84}$,[135,136] $Au_{329}(SR)_{84}$,[137,138] $[Ag_{374}(SR)_{113}Br_2Cl_2]$,[139] $Au_{333}(SR)_{79}$,[140] and $Au_{246}(SR)_{80}$ [141] were reported by different groups. There are also attempts to accurately probe the composition of plasmonic NPs using mass spectrometry.[142,143]

In the few past years, there have been immense advancements in analytic instrumentation, making it possible to study these precision materials in detail.[26,91,144–146,147] High-resolution mass spectrometry (HR MS) coupled with soft ionization can precisely determine the composition of the core and ligands as well as the charge states of the nanocluster.[55,148] Other advanced mass spectrometric (MS) techniques, like ion mobility MS (IM-MS)[97,149–153] and tandem MS (MS/MS),[19,154,155] are becoming increasingly powerful to understand the size, shape, and structural evolution. Single-crystal X-ray crystallography has made it possible to resolve the structures of several thiol (–SR)-capped nanoclusters, like $Au_{25}(SR)_{18}$,[134] $Au_{28}(SR)_{20}$,[156] $Au_{38}(SR)_{24}$,[157] $Au_{40}(SR)_{24}$,[158] $Au_{52}(SR)_{32}$,[159] $Au_{40}(SR)_{24}$,[160] $Au_{92}(SR)_{44}$,[159] $Au_{102}(SR)_{44}$,[131] $Au_{133}(SR)_{52}$,[161] $Ag_{44}(SR)_{30}$,[162] $Ag_{25}(SR)_{18}$,[163] $Ag_{29}(SR)_{12}$,[164] and more. Furthermore, with the development of hyphenated techniques, other inherent nanocluster properties, such as electron affinity (EA), ionization energy (IE), electronic transitions, *etc.*, are being studied in greater detail.[91] A few of the milestones in the development of noble metal cluster chemistry are briefly presented in Fig. 2.

2.4. Structural models

Various models have been proposed to understand the structure and stability of these nanoclusters.[9,41,129] When the 'divide and protect model',[114] which was one of the earliest, was put forward, no crystal structures were known for thiolate-protected noble metal nanoclusters. In 2008, Häkkinen *et al.* proposed the superatom complex (SAC), which was an extension of the superatom theory and was used in the case of gas-phase metal nanoclusters, to understand the stability of ligand-protected noble metal nanoclusters.[130] In 2013, Cheng *et al.* proposed the superatom network (SAN) model for some of the thiolate-protected noble metal nanoclusters.[165] They also proposed the superatom valence bond (SVB) model for non-spherical nanoclusters such as $Au_{38}(SR)_{24}$ for which the ordinary SAC model cannot be used for explaining the stability. In 2015, Natarajan *et al.* proposed a new structural model, namely the Borromean ring model,[166] for thiolate-protected noble metal nanoclusters wherein these nanoclusters are viewed as a single structural unit, *i.e.*, interlocked oligomeric metal–ligand rings in contrast to the 'divide and protect model' wherein nanoclusters possess a discrete core and staple units. According to this model, $Au_{25}(SR)_{18}$, for example, is viewed as three interlocked $Au_8(SR)_6$ rings surrounding the central Au atom. For the first time, a systematic method of precise naming of alloy nanoclusters and mixed-ligand nanoclusters based on this model was proposed. In 2016, Xu *et al.* proposed another structural model, namely the grand unified model (GUM) that successfully comprehended the structures of all the gold nanoclusters known by then.[167] Here, these gold nanoclusters are viewed as built up from triangular and tetrahedral elementary building blocks. An interesting suggestion based on this model is that the evolution of the gold cores in these nanoclusters cannot be viewed simply as the addition of an Au atom alone, but rather as built from these elementary building blocks.

2.5. Properties of metal nanoclusters

Soon after the crystal structures of $Au_{102}(SR)_{44}$ and $Au_{25}(SR)_{18}$ were resolved, attempts to understand the structure–property relations in these nanoclusters also commenced. For example, distinct electronic absorption bands of $Au_{25}(SR)_{18}$ were assigned to various electronic transitions within the molecular orbitals derived from the metal atoms and the ligands.[50,126] Several groups have studied the electrochemistry of various metal nanoclusters[168] and their alloys,[169–171] such as $Au_{25}(SR)_{18}$, $Au_{38}(SR)_{24}$, $Au_{67}(SR)_{35}$, $Au_{102}(SR)_{44}$, $Au_{144}(SR)_{60}$, $Au_{333}(SR)_{79}$ $Ag_xAu_{25-x}(SR)_{18}$ (x = 1–5), $M_2Au_{36}(SR)_{24}$ (M = Pd, Pt), *etc.*, further establishing the molecule-like electronic structures of these nanoclusters.[172,173] In 2008, distinct charge states of $Au_{25}(SR)_{18}$ were observed by a few research groups.[66,130] Electron paramagnetic resonance (EPR) spectroscopy of $Au_{25}(SR)_{18}$ was also reported subsequently.[66] Photoluminescence in gold nanoclusters was first reported by Wilcoxon *et al.* in 1998 [174] and subsequently by many other groups.[50,111,126,128] Photoluminescence was observed from protein-protected noble metal nanoclusters as well.[19] Nuclear magnetic resonance (NMR) spectra of $Au_{25}(SR)_{18}$ were reported by different groups.[67,175,176] In 2010, the structure of $Au_{38}(SR)_{24}$, another popular member of the thiolate-protected gold nanoclusters, was theoretically predicted by Lopez-Acevedo *et al.*,[44] and its crystal structure was revealed in the same year by Qian *et al.*[157] Chirality in thiolate-protected noble metal nanoclusters was first reported by Schaaff and Whetten in 2000.[177] In 2012, the first separation of enantiomers of $Au_{38}(SR)_{24}$ was achieved using chiral HPLC by Dolamic *et al.*,[178] which was a significant step toward understanding the chirality of nanoclusters. In 2015, the structural isomerism in $Au_{38}(SR)_{24}$ was observed by Tian *et al.*[179] Infrared and Raman spectroscopy of these nanoclusters were reported by Dolamic *et al.* and Varnholt *et al.*, in 2013 and 2014, respectively, revealing the distinct vibrational features of the staples of these nanoclusters.[180,181] Whereas most of these advance-

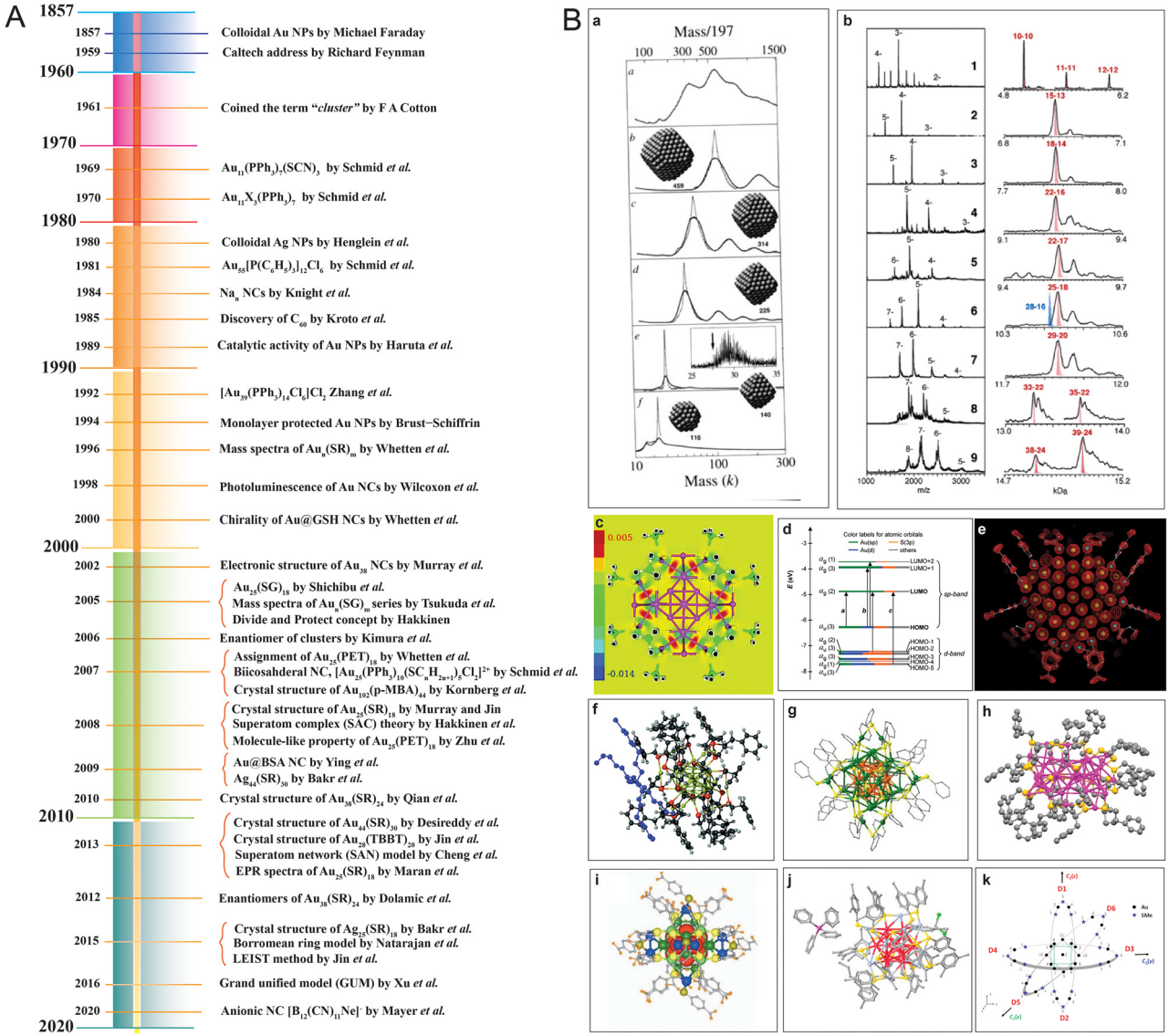

Fig. 2 (A) A representative timeline of the evolution of nanocluster science. (B) A few notable mentions from the nanocluster timeline, namely (a) mass spectra of $Au_n(SR)_m$, (b) mass spectra of $Au_n(SG)_m$ series, (c) divide and protect concept as visualized from the difference in electron density due to bonds, (d) Kohn–Sham (KS) orbital energy level diagram of $Au_{25}(SH)_{18}^-$, crystal structures of (e) $Au_{102}(p\text{-MBA})_{44}$, (f) $[N(C_8H_{17})_4][Au_{25}(SH)_{18}]$, (g) $Ag_{44}(4\text{-FTP})_{30}(PPh_4)_4$, (h) $Au_{38}(SR)_{24}$, (i) $Na_4Ag_{44}(MBA)_{30}$, and (j) $Ag_{25}(DMBT)_{18}$, and (k) Borromean rings diagram of $Au_{25}(SMe)_{18}$ nanocluster. Adapted from ref. a,[109] b,[113] c,[114] d[50,126] e,[131] f,[134] g,[291] h,[292] i,[162] j,[163] and k.[166] Copyright 1996 John Wiley and Sons. Copyright 2005, 2006, 2008, 2010, and 2015 American Chemical Society. Copyright 2007 American Association for the Advancement of Science. Copyright 2013 Springer Nature Group.

ments were centered around gold nanoclusters, the search for an atomically precise silver nanocluster was fruitful only in 2013 when Desireddy *et al.* reported the structure of $Ag_{44}(SR)_{30}$.[162] $Ag_{25}(SR)_{18}$, which is structurally and compositionally analogous to $Au_{25}(SR)_{18}$, was discovered in 2015 by Joshi *et al.*[163] Clusters of other metals and alloy nanoclusters composed of two, three and four elements have been reported.[10,182] Apart from thiolates, a wide variety of ligands, such as selenolates,[183–187] tellurolates, alkynes,[188,189] carbenes,[190] *etc.*, have also been used as protecting ligands for noble metal nanoclusters. For a comprehensive summary of the advancements in the field of thiolate-protected noble metal nanoclusters, please consult several additional references.[7,8,10–12,41,57,91,173,191–194]

3. Chemical reactivity of ligand-protected atomically precise metal clusters

The molecule-like nature of the physical properties of these nanoclusters is evident from the structural and spectroscopic studies discussed above. Recently, we have shown that these

nanoclusters exhibit molecule-like chemical reactivity as well. In the following sections, we discuss different aspects of their chemistry in detail.

3.1. Ligand exchange and ligand-induced transformations

Post-synthetic modification in particles is a versatile approach for the transformation in atomically precise nanoclusters in terms of compositional, morphological, and structural changes. Reactions of nanoclusters with structurally different ligands are another way to synthesize new nanoclusters. Substitution or exchange of ligands is one of the earliest reactions of such nanoclusters.[195]

Over the past two decades, monolayer-protected metal nanoclusters reacting with various ligands have produced nanoclusters with novel physical and chemical properties.[196] Murray *et al.* performed the first of such ligand-exchange reactions with thiol-protected gold nanoclusters.[197] Murray *et al.* also studied the mechanism of these ligand-exchange reactions in detail using mass spectrometry, NMR spectroscopy, and electrochemistry.[195,198] The rate of such reactions depends on the concentrations of both the nanocluster and the foreign ligand. The electron-donating and withdrawing nature of the functional groups on the ligands also governs the reaction rates. Using electrochemistry, Parker *et al.* showed that the electron-withdrawing ligands accelerate the exchange rate relative to electron-donating ligands.[199] Murray *et al.* observed that the ligand exchange is a second-order reaction.[200] Rate of reaction is determined by the bonding of incoming and outgoing ligands with metal, much like an associative mechanism. However, the rate is independent of the size of the nanoclusters. For example, both $Au_{38}(PET)_{24}$ and $Au_{140}(PET)_{53}$ showed similar rate constants during ligand exchange using various *p*-substituted aryl thiols.[201] The understanding of site selectivity and specificity of ligands in exchange reactions significantly improved with the availability of single-crystal structures of nanoclusters.

When noble metal nanoclusters react with foreign ligands, they undergo a transformation that leads to three types of ligand-exchange products. These products can result in the nanocluster with (i) retention of its structure and composition upon exchange, (ii) alteration in geometry while retaining its composition, or (iii) alteration in both structure and composition.

The initial reports on ligand-exchange reactions indicate that structure and composition of the nanocluster remain unaltered in the process. Murray *et al.* extensively studied the ligand-exchange reactions on $Au_{25}(PET)_{18}$ with different SR (where, R = Ph–CH_3, Ph–F, *etc.*), which resulted in $Au_{25}(SR)_{18-x}(SR')_x$ series (x = 1–12).[200,202,203] Partial ligand exchange was observed during the reaction of *p*-BBT (BBT = bromobenzenethiol) with $Au_{102}(p\text{-MBA})_{44}$ and $Au_{25}(PET)_{18}$ which led to the formation of $Au_{102}(p\text{-MBA})_{40}(p\text{-BBT})_4$ and $Au_{25}(PET)_{16}(p\text{-BBT})_2$, respectively.[204,205] In 2014, Abdulhalim *et al.* reported the ligand exchange on $Ag_{44}(4\text{-FTP})_{30}$ (FTP = fluorothiophenol) with various other aryl thiols such as MNBA (5-mercapto-2-nitrobenzoic acid), 4-NTP (NTP = nitrothiophenol), and 2-NT (NT = naphthalenethiol) which resulted in the formation of $Ag_{44}(SR)_{30}$ (where SR = MNBA/4-NTP/2-NT).[206] A second type of ligand exchange, referred to as ligand-induced isomerization, was reported in 2016 by Jin *et al.* upon the reaction of $Au_{28}(CHT)_{20}$ (CHT = cyclohexanethiol) with TBBT ligand (4-*tert*-butylbenzenethiol), in which the structure of the nanocluster changed while the composition remained unchanged.[207]

In 2008, Shibu *et al.* came up with the first report on post-synthetic modification of atomically precise Au_{25} nanoclusters *via* ligand exchange reaction.[195] Performing a ligand exchange with functionalized glutathione on the $Au_{25}(SG)_{18}$ nanocluster altered its optical and photoluminescence properties. These reactions have since found widespread application for modifying the chemical and other properties of nanoclusters through the introduction of new ligands to the parent clusters. Recently, ligand-exchange-induced structure transformation (LEIST) has become a rapidly developing technique in nanoclusters. In such reactions, when a foreign ligand is introduced, it can cause significant distortion of the core, resulting in both structural and compositional changes within the nanocluster. In 2013, Jin *et al.* introduced the term LEIST when they observed the transformation of $Au_{38}(SR)_{24}$ to $Au_{36}(SR')_{24}$ nanocluster through a ligand-exchange reaction. Jin *et al.* performed the ligand-exchange reaction on $Au_{38}(PET)_{24}$ with excess TBBT (TBBT = 4-*tert*-butylbenzenethiol) under thermal conditions, resulting in molecularly pure $Au_{36}(TBBT)_{24}$ in excellent yield.[208] The process of ligand exchange brings about a change in the structure of biicosahedral $Au_{38}(PET)_{24}$, transforming it into a truncated tetrahedral $Au_{36}(TBBT)_{24}$ with an FCC kernel. Interestingly, one of the first examples of an FCC-structured $Au_n(SR)_m$ nanocluster is $Au_{36}(TBBT)_{24}$. Zeng *et al.* established the universality of the LEIST method by reacting $Au_{25}(PET)_{18}$ with TBBT under thermal conditions, which led to the formation of $Au_{28}(TBBT)_{20}$.[156] The Jin group's discovery of the LEIST method led to the synthesis of numerous new nanoclusters.[209] Following this work, a large number of transformations was studied by different groups, such as conversions of $Au_{11}(PPh_3)_7Cl_3$ to $[Au_{25}(SR)_5(PPh_3)_{10}X_2]^{2+}$,[210] $Au_{15}(SG)_{13}$ to $Au_{16}(S\text{-Adm})_{12}$,[211] $Au_{18}(S\text{-c-}C_6H_{11})_{14}$ to $Au_{21}(S\text{-Adm})_{15}$,[212] *etc.*, which proved the method to be versatile for making new structures. Furthermore, similar structural changes were observed in silver nanoclusters, and the mechanisms underlying these changes were investigated in detail. Bakr *et al.* showed the reversible conversion between $Ag_{25}(2,4\text{-DMBT})_{18}$ (DMBT = dimethylbenzenethiol) and $Ag_{44}(4\text{-FTP})_{30}$ (FTP = fluorothiophenol).[213] Upon reaction with 2,4-DMBT, $Ag_{44}(4\text{-FTP})_{30}$ underwent a disproportionation reaction to form smaller sized $Ag_{25}(4\text{-FTP})_1(2,4\text{-DMBT})_{17}$ and bigger sized $Ag_{46-50}(4\text{-FTP})_{4-9}(2,4\text{-DMBT})_{21-26}$. After complete ligand exchange, other less stable nanoclusters transformed to more stable $Ag_{25}(2,4\text{-DMBT})_{18}$. On the other hand, the conversion of $Ag_{25}(2,4\text{-DMBT})_{18}$ to $Ag_{44}(4\text{-FTP})_{30}$ occurred *via* dimerization of $Ag_{25}(2,4\text{-DMBT})_{18}$ followed by a rearrangement pathway. A similar mechanism was observed during the conversion of $Ag_{35}(SG)_{18}$ to $Ag_{44}(4\text{-FTP})_{30}$.[214] Khatun *et al.* showed a distinctly

different mechanistic pathway during the transformation of $Ag_{59}(2,5\text{-DCBT})_{32}$ (DCBT = dichlorobenzenethiol) to $Ag_{44}(2,4\text{-DCBT})_{30}$, $Ag_{25}(2,4\text{-DMBT})_{18}$ and $Ag_{29}(1,3\text{-BDT})_{12}(PPh_3)_4$ (BDT = benzenedithiol) upon reaction with 2,4-DCBT, 2,4-DMBT and 1,3-BDT/PPh_3, respectively (Fig. 3).[215] In the presence of incoming thiol ligands, $Ag_{59}(2,5\text{-DCBT})_{32}$ dissociated completely into smaller nanoclusters and thiolates instead of ligand exchange. Then, these smaller nanoclusters and thiolates recombined and rearranged to form the final product. The nature of the thiolate ligand plays an important role in determining the structure and composition of the product nanoclusters. Khatun *et al.* also reported the synthesis of $MAg_{28}(1,3\text{-BDT})_{12}(PPh_3)_4$ from $MAg_{24}(2,4\text{-DMBT})_{18}$ *via* the LEIST method. Recently, a phosphine-protected nanocluster $Ag_{18}(PPh_3)_{10}H_{16}$ synthesized by Bakr *et al.* was observed as a very good precursor for the LEIST reaction (Fig. 4).[216] Bodiuzzaman *et al.* synthesized two new nanoclusters, $Ag_{46}(DMBT)_{24}(PPh_3)_8$ and $Ag_{40}(DMBT)_{24}(PPh_3)_8$ *via* the LEIST method, using $Ag_{18}(PPh_3)_{10}H_{16}$.[217] Manju *et al.* synthesized NIR-emitting $[Ag_{34}S_3(SBB)_{20}(CF_3COO)_6]^{2+}$ nanocluster from $Ag_{18}(PPh_3)_{10}H_{16}$ upon reacting it with tertiary-butylbenzylthiol (SBB).[218] Upon reacting $Ag_{18}(PPh_3)_{10}H_{16}$ with 2-pyrene imine thiol (2-PIT), Jana *et al.* synthesized a new dual-emitting nanocluster, $[Ag_{35}(2\text{-PIT})_7(PPh_3)_7@(H_2O)]^{3+}$.[219] Kang and Zhu published an extensive review on the evolution of the LEIST methodology and its application.[220]

Ligand exchange is an effective strategy to improve the physical and chemical properties of nanoclusters. The method has largely been used to enhance the emission quantum yield (QY) of several non-luminescent or feebly luminescent nano-

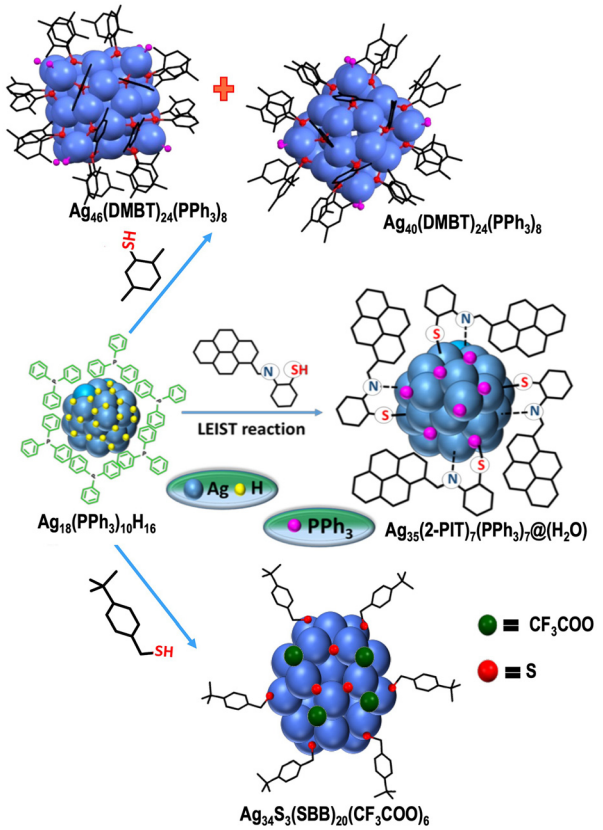

Fig. 4 Formation of $[Ag_{34}S_3(SBB)_{20}(CF_3COO)_6]^{2+}$, $[Ag_{35}(2\text{-PIT})_7(PPh_3)_7@(H_2O)]^{3+}$, $Ag_{46}(DMBT)_{24}(PPh_3)_8$ and $Ag_{40}(DMBT)_{24}(PPh_3)_8$ from $Ag_{18}(PPh_3)_{10}H_{16}$ *via* LEIST method. Adapted from ref. 217. Copyright 2019 John Wiley and Sons.

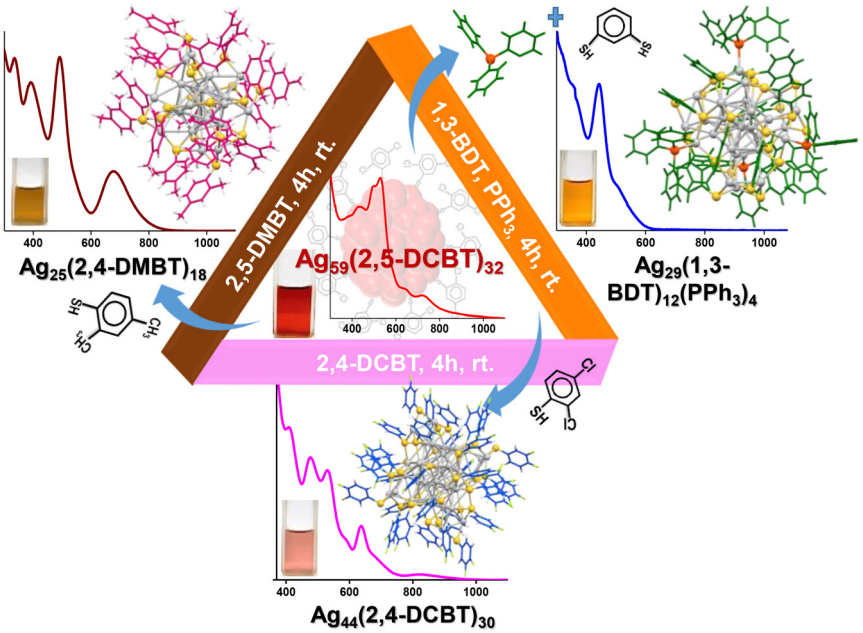

Fig. 3 Schematic representation of ligand exchange-induced conversion of $Ag_{59}(2,5\text{-DCBT})_{32}$ to $Ag_{44}(2,4\text{-DCBT})_{30}$, $Ag_{25}(2,4\text{-DMBT})_{18}$ and $Ag_{29}(1,3\text{-BDT})_{12}(PPh_3)_4$ after the reaction with 2,4-DCBT, 2,4-DMBT and 1,3-BDT/PPh_3, respectively, under ambient conditions. Adapted from ref. 215. Copyright 2017 Royal Society of Chemistry.

clusters. Jin *et al.* showed an improvement in photoluminescence (PL) intensity while preserving the composition of $Au_{25}(SR)_{18}$.[221] They found higher QY for $Au_{25}(PET)_{18}$ (PET = 2-phenylethanethiol) than for $Au_{25}(DDT)_{18}$ (DDT = dodecanethiol) and $Au_{25}(HT)_{18}$ (HT = hexanethiol). Later on, the PL intensity of $Au_{25}(PET)_{18}$ enhanced 6.5 fold on using NAP (NAP = 2-(naphthalen-2-yl)ethanethiolate) ligand instead of PET.[222] Kim *et al.* showed enhancement in PL intensity of $Au_{36}(TBBT)_{24}$ (TBBT = *tert*-butylbenzenethiol) by partial ligand exchange using CPT (CPT = cyclopentanethiol) ligand.[223] Similar to gold nanoclusters, ligand engineering in silver nanoclusters also led to the enhancement of the PL QY. Khatun *et al.* found structure-conserved ligand exchange in $Ag_{29}(BDT)_{12}(PPh_3)_4$ (BDT = 1,3-benzenedithiol) using various diphosphine ligands such as DPPM (1,1-bis(diphosphino) methane), DPPE (1,2-bis(diphosphino)ethane) and DPPP (1,3-bis(diphosphino)propane) which resulted in the increment of PL QY, as shown in Fig. 5.[224] Among these nanoclusters, $Ag_{29}(BDT)_{12}(DPPP)_4$ exhibited highest PL QY which is 30 fold higher than that of $Ag_{29}(BDT)_{12}(PPh_3)_4$. The PL intensity can also be modified by the structure, transformed due to ligands. Such an example is the conversion of $Pt_1Ag_{24}(SR)_{18}$ to $Pt_1Ag_{28}(SAdm)_{18}(PPh_3)_4$ (SAdm = adamentanethiol) which displayed 50-fold higher PL QY than the parent nanocluster.[225] Other properties such as chirality is introduced in nanoclusters using the ligand exchange method.[226,227] Bürgi *et al.* introduced chirality in $Au_{38}(PET)_{24}$ nanocluster by partial ligand exchange using chiral bidentate thiol, BINAS (BINAS = 1,1′-binaphthyl-2,2-dithiol).[228]

3.2. Reactions with metal ions

The interaction of a metal ion with the noble metal nanocluster is reflected in the changes observed in the absorption and emission spectra of the nanocluster. Some metal nanoclusters are known to be highly fluorescent compared to their bulk counterparts. Also, the post-synthetic metal-exchange reactions with noble metal nanoclusters are an important method for the preparation of alloy nanoclusters. Of all the known metal-exchange methods, galvanic reduction is one of the most efficient approaches for the preparation of multimetallic alloy nanoclusters.

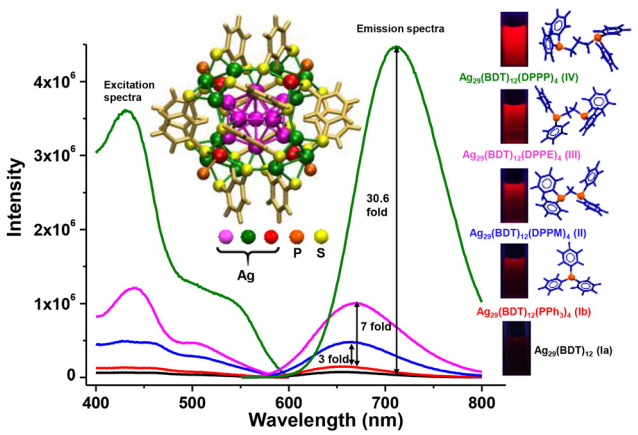

Fig. 5 Excitation and emission spectra of $Ag_{29}(BDT)_{12}$ and $Ag_{29}(BDT)_{12}(P)_4$ where P = PPh_3, DPPM, DPPE, DPPP. A systematic enhancement of PL intensity is observed. Photographs of nanoclusters under UV light are also shown. Reproduced from ref. 224. Copyright 2018 Royal Society of Chemistry.

Metal ion-induced alteration in the fluorescence of nanoclusters is one of the most used strategies for sensing heavy metal ions, like Hg^{2+}, Cu^{2+}, As^{3+}, Cr^{3+}, Pb^{2+}, *etc.*[75] In 2007, Habeeb *et al.* were the first to report the reactivity of $Au_{25}SG_{18}$ nanocluster to $AuCl_4^-$.[229] The $Au_{25}SG_{18}$ nanocluster underwent an instantaneous decomposition in the presence of $AuCl_4^-$ ions to form an insoluble gold–glutathione coordination polymer (Au_nSG_m). The characteristic absorption features of $Au_{25}SG_{18}$ nanocluster get quenched immediately after addition $AuCl_4^-$ ions due to the formation of Au(I) – glutathione complex. Upon reaction with other metal ions, such as Ag^+, Fe^{3+}, Cu^{2+}, Ni^{2+}, Cd^{2+}, Zn^{2+} and Sr^{2+}, the $Au_{25}SG_{18}$ nanocluster decomposes but at a slower rate. The net reaction of $Au_{25}SG_{18}$ nanocluster – Au^{3+} ion can be represented as an electron-transfer process where the electrons from the nanocluster core reduce $AuCl_4^-$ to $AuCl_2^-$ ions.

Mercury (Hg) is one of the most toxic heavy metals. Bootharaju and Pradeep reported that the $Ag_{7,8}(MSA)_{7,8}$ nanocluster (MSA = mercaptosuccinic acid) can act as a Hg and other heavy metal scavenger.[230] In the reaction medium, the silver nanocluster interacts preferentially through its core and the carboxylate group of mercaptosuccinic acid (MSA) ligand depending upon the concentration of Hg^{2+} ion. The $Ag_{7,8}(MSA)_{7,8}$ nanocluster undergoes luminescence quenching as it interacts with Hg^{2+}. To understand the scavenging property of the $Ag_{7,8}(MSA)_{7,8}$ nanocluster, it is important to note that the redox potentials of Ag^{1+}/Ag^0 decrease with the particle size compared with the bulk metal, which is +0.79 V, whereas it is +0.8 V for the interacting metal ion (Hg^{2+}/Hg^0). The net cell electromotive force (*emf*) for the reduction of Hg^{2+} by the silver nanocluster is positive. The alumina-loaded $Ag_{7,8}(MSA)_{7,8}@Al_2O_3$ nanocluster can be used quantitatively for Hg^{2+} removal from contaminated water. Later on, from the same group, Chakraborty *et al.* went ahead to report the selective reaction of $Ag_{25}SG_{18}$ nanocluster with Hg^{2+} ion. The chemical interaction of $Ag_{25}SG_{18}$ nanocluster and Hg^{2+} ion resulted in the formation of Ag_3Hg_2 alloy (*paraschachnerite* with an orthorhombic crystal structure), as observed with the appearance of new blue-shifted features in the optical absorption spectra (Fig. 6). XPS studies show that the $Ag_{25}SG_{18}$ nanocluster – Hg^{2+} ion reaction is a redox process which involves oxidation of Ag^0 to Ag^+ and reduction of Hg^{2+} to Hg^0. The luminescent $Ag_{25}SG_{18}$ nanocluster can act as a sensing material, as it undergoes fluorescence quenching upon interaction with Hg^{2+} ions with a limit of detection of 1 ppb.

Another heavy metal present in drinking water is Cu^{2+}, which has a permissible limit of 1.3 ppm in drinking water as set by the U.S. Environmental Protection Agency (EPA). Glutathione (GSH) is a natural tripeptide in amino acids, such as cysteine, glutamic acid, and glycine. GS-protected gold

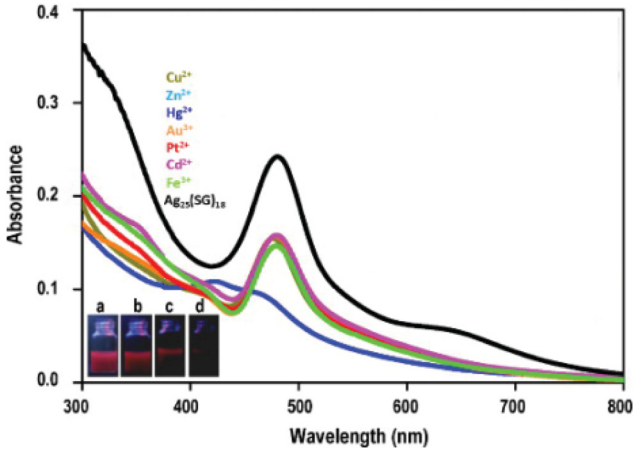

Fig. 6 Optical absorption spectra of the $Ag_{25}SG_{18}$ nanocluster solution on addition of different metal ions. Under UV excitation, images corresponding to fluorescence quenching of (a) phase transferred nanocluster and on the addition of (b) 1 ppm, (c) 2 ppm, and (d) 10 ppm of Hg^{2+}. Adapted from ref. 290. Copyright 2012 Elsevier.

nanoclusters are biocompatible and have strong near-IR fluorescence emission compared with other non-aqueous $Au_n(SR)_m$, making them a popular candidate for developing biological and heavy metal sensors. Back in 2009, fluorescent Au@GS NPs made a debut as a highly selective Cu^{2+} sensor, which is a classic example of aggregation-induced fluorescence quenching.[231] Later on, efforts were undertaken by George *et al.* for sensing Cu^{2+} ions using thiolate-protected gold nanoclusters.[34] This work involved a GS-protected Au_{15} nanocluster encapsulated in cyclodextrin (CD) cavities (denoted by Au_{15}@CD). The sensor material is prepared by loading the Au_{15}@CD nanocluster onto a freestanding film of chitosan. This nanocluster composite material is a bright luminescent film under UV light. Upon exposing the nanocluster composite material to Cu^{2+} ions, luminescence quenching happens which is selective to Cu^{2+} ion concentration. A change in emission maximum was observed in the PL spectra of the material before and after its exposure to Cu^{2+} ions. The sensing specificity of the nanocluster composite material towards Cu^{2+} ion was studied using XPS analysis, which suggested a reduction of Cu^{2+} to Cu^{1+}/Cu^0 by the glutathione ligand or the Au_{15} core. The reported limit of detection of the GS-protected-Au_{15}@CD nanocluster composite material is 1 ppm of Cu^{2+} ion present in the medium. Zhang *et al.* reported the application of water-soluble GS-protected gold nanoclusters in Cu^{2+} sensing with a limit of detection of 86 nM.[72] The quenching of the fluorescence is attributed to the carboxylic group in GSH-ligand, which is a chelating agent with a high affinity and selectively towards Cu^{2+} ion over other metal ions, like Hg^{2+} and Pb^{2+}, present in the medium. Krishnadas *et al.* reported a highly luminescent MSA-protected Ag–Au bimetallic nanocluster (denoted as AgAu@MSA) material as a Cu^{2+} sensor. Initially, the preparation of the AgAu@MSA nanocluster involved a galvanic reduction of polydispersed Ag NPs by Au^{I}-MSA thiolates. A methanolic solution of the AgAu@MSA nanocluster undergoes immediate luminescence quenching selectively upon interaction with Cu^{2+} even in the presence of other metal ions. The mechanism of metal-induced fluorescence quenching of the nanocluster was investigated using XPS, and it was concluded that the Cu^{2+} ion interacts with the AgAu metal core of the nanocluster. The nanocluster–metal ion interaction is a redox process; the AgAu metal core reduces the Cu^{2+} ion to Cu^{1+}/Cu^0, while it gets oxidized in the process.

In the following part, we will focus on the metal-exchange reactions of noble metal nanoclusters resulting in alloy nanoclusters. As per the galvanic theory, the metal ion with a higher reduction potential replaces another metal with a lower reduction potential, and subsequently, it gets reduced (Fig. 7A). The reduction potential of metals in decreasing order is $Fe^{2+} > Cd^{2+} > Co^{2+} > Ni^{2+} > [Au\ NCs] > Cu^{2+} > Hg^{2+} > Ag^{1+} > Pd^{2+} > Pt^{2+} > Au^{1+}$.[232,233] Using the galvanic replacement method, various multimetallic noble metal alloy nanoclusters are formed. One such example is the Au-incorporated $Ag_{24}Au(DMBT)_{18}$ nanocluster derived from $Ag_{25}(DMBT)_{18}$ studied by Bootharaju *et al.*, where the reduction potentials of Ag^+/Ag and Au^+/Au are 0.080 and 1.69 V, respectively (Fig. 7C(a)).[234] The structure of the bimetallic $Ag_{24}Au(DMBT)_{18}$ nanocluster is analogous to its monometallic counterpart with enhanced stability and photoluminescence. The reaction of $PdAg_{24}(SR)_{18}$ and Au-salt was found to proceed *via* trimetallic $PdAuAg_{23}(SR)_{18}$ nanocluster intermediate and finally resulting in a replacement product, the $AuAg_{24}(SR)_{18}$ nanocluster. But the Au ionic reaction with the structurally equivalent $PtAg_{24}(SR)_{18}$ nanocluster led to the formation of $Au_2PdAg_{22}(SR)_{18}$ nanocluster. Later, Kang *et al.* reported dopant-dependent shape-controlled galvanic exchange reactions.[235] The Au-doping in a $PtAg_{24}(DMBT)_{18}$ nanocluster with the precursors Au-DMBT and $AuBrPPh_3$ resulted in the formation of trimetallic nanoclusters with shape-unaltered $PtAu_xAg_{24-x}(DMBT)_{18}$ and altered $Pt_2Au_{10}Ag_{13}(PPh_3)_{10}Br_7$ nanoclusters, respectively (Fig. 7C(b)). Similarly, multimetallic $PtCu_xAg_{28-x}(BDT)_{12}(PPh_3)_4$ and $Pt_1Ag_{12}Cu_{12}Au_4(S\text{-}Adm)_{18}(PPh_3)_4$ nanoclusters were prepared using the galvanic exchange method.[236] Bootharaju *et al.* studied the metal-exchange reaction between $MAg_{24}(SR)_{18}$ (M = Pd/Pt) and $AuPPh_3Cl$ salt, using mass spectrometry (Fig. 7C(c)).[237] Likewise, using the templated galvanic metal-exchange route, a highly stable $Au_{5.34}Ag_{44.66}(Dppm)_6(TBBM)_{30}$ (Dppm = bis(diphenylphosphino)methane and TBBM = 4-*tert*-butylbenzyl mercaptan) nanocluster was prepared from $Ag_{50}(Dppm)_6(TBBM)_{30}$ (Fig. 7C(d)).[238]

An anti-galvanic reaction (AGR) defies the classical galvanic reduction (GR) as the metal ions get reduced by the less reactive (or more noble) metal (Fig. 7B). The driving force for an anti-galvanic reaction can be explained in terms of the difference in the redox potential of the participating entities. In 1985, Plieth proposed a theory on the relationship between the electrode potential of metal nanoparticles and their particle diameter.[239] Theoretically, bulk metals (M_{bulk}) can be transformed into small metal particles (M_{NP}) by dissolving into metal ions (M^+) and then redepositing as particles. The

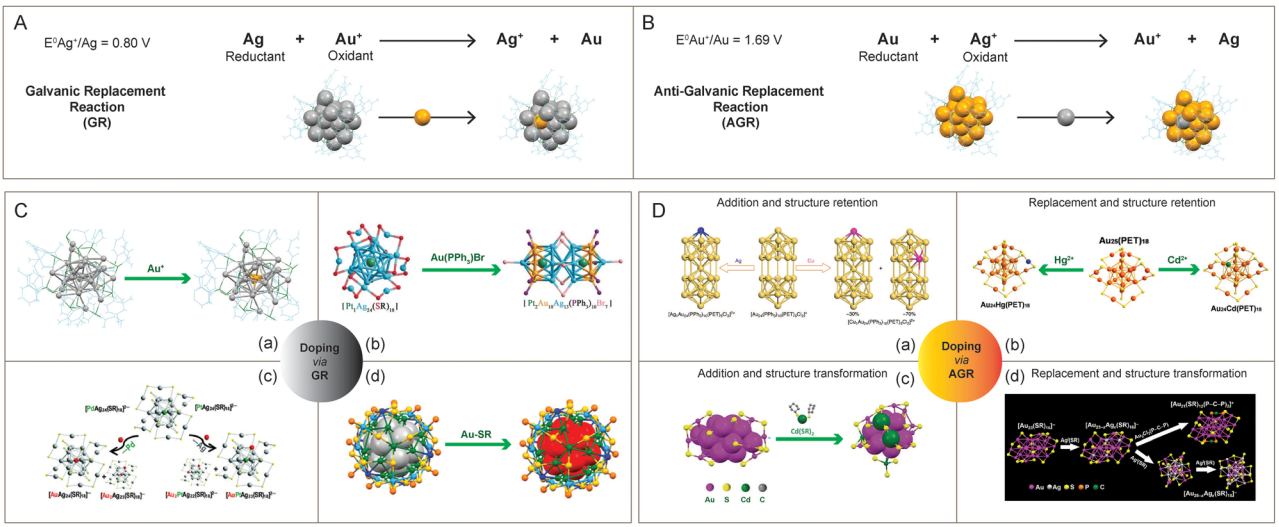

Fig. 7 Schematic representation of (A) galvanic replacement and (B) anti-galvanic replacement reaction from the context of doping in $Ag_{25}(SR)_{18}$ and $Au_{25}(SR)_{18}$, respectively. Examples showing the preparation of alloy nanoclusters using (C) galvanic and (D) anti-galvanic reaction routes. Reproduced with permission from ref. C-a,[234] b,[236] c,[237] and d,[238] and D-a,[246] b,[248] c,[251] and d.[249] Copyright 2015 and 2017 American Chemical Society. Copyright 2016 and 2018 John Wiley and Sons. Copyright 2016 Royal Society of Chemistry. Copyright 2017, Springer Nature Group. Copyright 2019 National Academy of Sciences.

reduction of bulk metal (M_{bulk}) into metal nanoparticles (M_{NP}) can be described by the electrochemical cell reaction,[239]

$$M_{bulk} \rightarrow M^{+}(aq) + ze^{-}$$

$$M^{+}(aq) + ze^{-} \rightarrow M_{NP}(s)$$

Plieth states that the standard reduction potential of a small metal particle undergoes a negative shift, as expressed in the following equation,[239]

$$\mu_d = \mu_b - \left(\frac{2M}{zF}\right)\frac{\gamma}{r}$$

where, μ_d and μ_b are the reduction potentials of metal NP and electrode of the same metal, respectively. The other terms are molar mass (M), specific mass (ρ), number of electrons (z), Faraday's constant (F), surface free energy (γ), and NP radius (r). Later, Zamborini *et al.* and Henglein *et al.* experimentally demonstrated a significant negative shift in the electrode potentials of Ag[87] and Au NPs[240] having sizes below 4 nm.

The ultrasmall-sized noble metals nanoclusters have been recently emerging as interesting candidates for anti-galvanic reactions.[232,241] The anti-galvanic reaction route provides a more facile and milder method towards alloying with a better control over the composition, structure, and properties of the nanoclusters. Choi *et al.* reported the first anti-galvanic reaction in nanoclusters with the alloying of $[Au_{25}(PET)_{18}]$ nanocluster.[242] The $[Au_{25}(PET)_{18}]^{-}$ nanocluster upon reaction with Ag^{+} ion resulted in a bimetallic $[Au_{24}Ag(PET)_{18}]^{-}$ nanocluster. From the electrochemical series, it is known that Au is less reactive than Ag, and it was anticipated that the reduction of Au(III) by Ag metal is facile in the ambient conditions but the opposite is not. In 2012, Wu studied the reaction of $Au_{25}(PET)_{18}$ with Ag^{+} and Cu^{2+} ions resulting in bimetallic products as characterized using matrix-assisted laser desorption/ionization time of flight mass spectrometry (MALDI-TOF MS) and XPS.[232] Ag^{+} ions failed to react with 2–3 nm Au NPs, thereby establishing $Au_{25}(PET)_{18}$ nanoclusters as a unique candidate towards anti-galvanic reaction. The thiolate (–SR) ligand coverage on the nanocluster surface plays a pivotal role in the anti-galvanic reactions. As the ligand attaches to the metal surface, it gains a partial negative charge which further assists in the reduction of less noble ions, like, Ag^{+} and Cu^{2+}. Here, the anti-galvanic reaction is catalyzed by the highly reactive metal atom on the nanocluster surface. The AGR products are influenced by monolayers on the nanocluster surface. For instance, Wu *et al.* demonstrated that when exposed to silver ion precursors (such as $AgNO_3$, Ag-PET, Ag-EDTA, and Ag-DTZ; where EDTA stands for ethylenediamine tetraacetic acid disodium salt and DTZ for dithiazone), $Au_{25}(PET)_{18}$ reacts and forms various Ag–Au alloy nanoclusters.[243] However, $Au_{25}(SG)_{18}$ does not exhibit any reaction with Ag^{+} ions.[244]

Using anti-galvanic reaction routes, gold nanoclusters can be alloyed by a heteroatom addition or replacement that also involves a retention or an alteration of the structural framework.[241]

Here are a few examples of heteroatom addition with retention of the initial nanocluster structural framework. The reaction between $Au_{25}(PET)_{18}$ and $AgNO_3$ in acetonitrile results in the formation of $Au_{25}Ag_2(PET)_{18}$ nanocluster as a major product.[245] The incoming Ag-atoms, instead of replacing Au-atoms, get added to the $Au_{25}(PET)_{18}$ nanocluster structure. Upon comparison with the $Au_{25}(PET)_{18}$ nanocluster, the Ag-added species, $Au_{25}Ag_2(PET)_{18}$, has a ~3.5-fold enhancement in QY while no change was seen in the Ag-replaced species, $Au_{25-x}Ag_x(PET)_{18}$ (x = ~3). Wang *et al.* observed that a foreign Ag-atom can squeeze into the hollow site of the $Au_{24}(PPh_3)_{10}(PET)_5Cl_2$ nanocluster without altering its compo-

sition or structure (Fig. 7D(a)).[246] Other popular examples of metallic replacement with the retention of starting nanocluster structure are Ag, Pt, and Pd-doped $Au_{38}(PET)_{24}$, Ag-doped $Au_{36}(TBBT)_{24}$, Cu and Ag-doped $Au_{144}(PET)_{60}$.[247] In 2015, Liao *et al.* synthesized $Au_{25}Hg_1(PET)_{18}$ and $Au_{25}Cd_1(PET)_{18}$ from $Au_{25}(PET)_{18}$ using an anti-galvanic reaction (Fig. 7D(b)).[248] The single-crystal X-ray diffraction of $Au_{25}Hg_1(PET)_{18}$ revealed the structural similarity with $Au_{25}(PET)_{18}$ where one of the outer-shell Au-atoms is replaced by a Hg-atom, while for the $Au_{25}Cd_1(PET)_{18}$ structure, the Cd-atom replaces the Au-atom to occupy the central position (Fig. 7B).

Jin *et al.* pioneered alloying methods where the heteroatomic replacement initiates a structural transformation. Li *et al.* studied the Ag-doping-induced transformation of the $Au_{23}(CHT)_{16}$ (CHT = cyclohexanethiolate) nanocluster into $Au_{25-x}Ag_x(CHT)_{18}$ (Fig. 7D(d)).[249] The alloying reaction between $Au_{23}(CHT)_{16}$ and Ag(I)-CHT proceeds through a two-step metal-exchange route: (i) $Au_{23}(CHT)_{16}$ is initially converted to a $Au_{23-x}Ag_x(CHT)_{16}$ ($x \sim 1$) intermediate, and (ii) then it is allowed to grow into $Au_{25-x}Ag_x(CHT)_{16}$ ($x \sim 4$), with Ag sitting at the icosahedral inner shell.[250] Zhu *et al.* reported another method of synthesis of the bimetallic nanocluster involving a non-replacement of the heteroatom along with a structural transformation. The $Au_{20}Cd_4(SH)(CHT)_{19}$ nanocluster was prepared from $Au_{23}(SR)_{16}$ using the anti-galvanic reaction (Fig. 7D(c)).[251] The starting $Au_{23}(SR)_{16}$ nanocluster is known to have an Au_{15} bi-capped cuboctahedron-based kernel, protected by two $Au_3(SR)_4$ trimeric and $Au(SR)_2$ monomeric staples along with four simple bridge –SR– ligands.[252] Structural similarity of Au_{25} and $Au_{20}Cd_4(SH)(CHT)_{19}$ nanocluster system was found to be composed of a centered icosahedral Au_{13} and $Au_{11}Cd_2$ kernel, respectively. The introduction of two Cd-atoms distorts the Au_{13} kernel of Au_{25}. The resulting nanocluster structure consists of a distorted central icosahedral $Au_{11}Cd_2$ kernel with the capping of two non-equivalent trimeric staples, one dimeric staple, two monomeric staples, four bridging thiolates (–SR–), and one CdSH unit. Li *et al.* reported Cd-addition to the $Au_{22}(SAdm)_{16}$ (SAdm = 1-adamantanethiol) nanocluster (bioctahedral Au_{10} kernel), which resulted in a structurally transformed $Au_{22}Cd_1(SAdm)_{16}$ nanocluster (cuboctahedral $Au_{12}Cd_1$ kernel).[253] Using the reaction between $Cl@Ag_{14}$ and AgClO, Hau *et al.* introduced the metal core enlargement in nanoclusters, leading to the formation of bigger $Cl_6Ag_8@Ag_{30}$.[116] Recent investigations have shown that carboxylate ligands on the surface of Ag nanoclusters provide ligand–shell flexibility, inducing structural modifications in the NCs due to differential coordination of Ag between carboxylate and thiol/alkyl moieties.[254,255] For example, monocarboxylate and dicarboxylate ligand triggers structural transformations $Mo_6O_{22}@Ag_{44} \rightarrow Mo_8O_{28}@Ag_{50}$ (ref. 254) and $Ag_{54} \rightarrow Ag_{28}$, (ref. 255) respectively.

3.3. Reactions with halocarbons

The studies of the reaction of halocarbons with noble metal NPs opened up a new direction in nanocluster chemistry. Nair and Pradeep reported that citrate-capped Ag and Au NPs possess catalytic property for the destruction of halocarbons, resulting in the formation of metal halides and amorphous carbon. This was the first time such properties had been reported.[256] The halocarbon, CCl_4, upon reaction with an alcoholic solution of Ag and Au NPs resulted in the formation of AgCl and $AuCl_3$, respectively, along with an amorphous carbon residue. This reaction was able to completely mineralize halocarbons like choloro, fluoro, and bromocarbons. Later, Bootharaju and Pradeep identified a pesticide degradation pathway using the citrate-capped Ag and Au NPs.[257] Here, chlorpyrifos (CP), an organophosphorothioate pesticide, was used as the model pesticide. After reacting with CP, optical absorption spectroscopy showed a red shift in the surface plasmon of Ag NP, and transmission electron microscopic (TEM) analysis revealed aggregation. Upon reaction with the unsupported and alumina-supported Ag and Au NP, the CP degrades into less toxic by-products like 3,5,6-trichloro-2-pyridinol (TCP) and diethyl thiophosphate (DETP), which was established using mass spectrometric studies. The proposed mechanisms involve steps like: (i) first, the CP binds to the NP surface through an $Ag_n^+ \leftarrow S$ bond, (ii) P–O cleavage, (iii) nucleophilic H_2O attack at the electrophilic P site, and (iv) finally, electron withdrawal from $Ag_n^+ \leftarrow N$ and $Ag_n^+ \leftarrow S$ bonds resulting the formation of stable TCP and DETP compounds. The Ag NPs were found to have better catalytic performance over Au NPs. When reacting with CP, the unsupported Ag@citrate NPs tend to aggregate, while the alumina-supported Ag NPs do not. This makes the latter more efficient for water purification, and reusable.

In 2013, Bootharaju *et al.* reported the degradation of halocarbons like CCl_4, $C_6H_5CH_2Cl$, and $CHCl_3$, using atomically precise Ag_9MSA_7 nanoclusters.[258] The reaction products, AgCl, CCl_3COOH, amorphous carbon, and acetone, were characterized using XRD, Raman, infrared, optical absorption, X-ray photoelectron spectroscopy, and mass spectrometry. To increase the miscibility of halocarbons like CCl_4 in the reaction mixture, isopropyl alcohol (IPA) was used. The precipitate is amorphous carbonaceous material with a graphitic structure, while the supernatant contains acetone from oxidation of IPA. The proposed mechanism (Fig. 8) involves an initial adsorption of IPA and CCl_4 on the nanocluster surface, which in turn catalyses the oxidation of IPA into acetone and activation of the C–Cl bond of the CCl_4. The surface activities initiate a series of electron transfer reactions like release of H^+ and Cl^- ions to the medium, making it acidic, Cl^- ions replacing the MSA ligands, oxidation of Ag^0 to Ag^+, and finally, mineralization of CCl_4.

3.4 Supramolecular chemistry of metal nanoclusters

The supramolecular chemistry of nanoclusters is an emerging area of research which also highlights the molecular nature of atomically precise nanoclusters. The organic ligands protecting the metal core of the nanocluster can interact with suitable molecules by weak supramolecular interactions. Such interactions include π–π, C–H···π, van der Waals and electrostatic interactions. Moreover, metallophilic interactions of the nano-

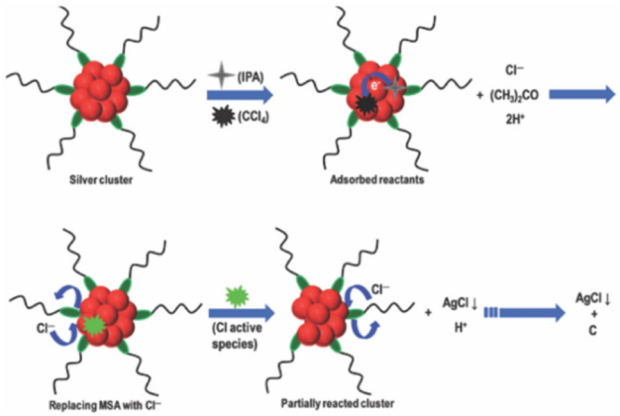

Fig. 8 Schematic representation of the proposed mechanism for degradation of halocarbons, like CCl_4, by Ag nanocluster. Adapted from ref. 258. Copyright 2013 Royal Society of Chemistry.

cluster core also play an active role in controlling the interactions. Such interactions have been the major driving force in controlling the crystal packing of the nanoclusters. Recently, such interactions have also been explored with other molecules. Mathew *et al.* reported interaction between $Au_{25}SBB_{18}$ (SBB = 4-(*t*-butyl)benzyl mercaptan) and cyclodextrins (CDs), which showed that the SBB ligands were encapsulated in the cavity of CDs, forming inclusion complexes of the nanocluster with CDs.[259] Chakraborty *et al.* reported host–guest complexes of nanoclusters and fullerenes.[260] Such interactions were largely dependent on the geometrical compatibility of the two molecules for forming the adducts and further assisted by weak supramolecular interactions. A range of such complexes can be made depending on the structure of the nanoclusters. $Ag_{29}(BDT)_{12}$ nanocluster can capture C_{60} molecules on its surfaces, forming adducts such as $[Ag_{29}(BDT)_{12}(C60)_n]^{3-}$ (n = 1–9). Structures of $[Ag_{29}(BDT)_{12}(C_{60})_4]^{3-}$ and $[Ag_{29}(BDT)_{12}(C_{60})_8]^{3-}$ are presented in Fig. 9A(a), which reveals that C_{60} molecules are captured on tetrahedral sites on the nanocluster surface, assisted by interactions with the BDT ligands. Similarly, $Ag_{25}(DMBT)_{18}^-$ and $Au_{25}(PET)_{18}^-$ nanoclusters also formed adducts with fullerenes.[261] Due to a different geometrical structure of $M_{25}(SR)_{18}^-$ nanoclusters compared with that of $[Ag_{29}(BDT)_{12}]^{3-}$ nanocluster, the nature of the host–guest adducts with fullerenes were also different in the two cases. $Ag_{25}(DMBT)_{18}^-$ and $Au_{25}(PET)_{18}^-$ nanoclusters formed aggregates with fullerenes as shown in Fig. 9A(b), and these aggregates were actually dimeric, trimeric, or polymeric adducts of the nanoclusters. Supramolecular interactions of nanoclusters with crown ethers have also been observed, and such complexes were crystallized.[262] Crown ethers were captured in the crystal lattice of Ag_{29} nanoclusters, forming lattice inclusion compounds, as shown in Fig. 9B. Such interactions also resulted in a change in the emission properties compared to the crystals of parent nanocluster. The chemical reactivity of the nanoclusters with other molecules also leads to the emer-

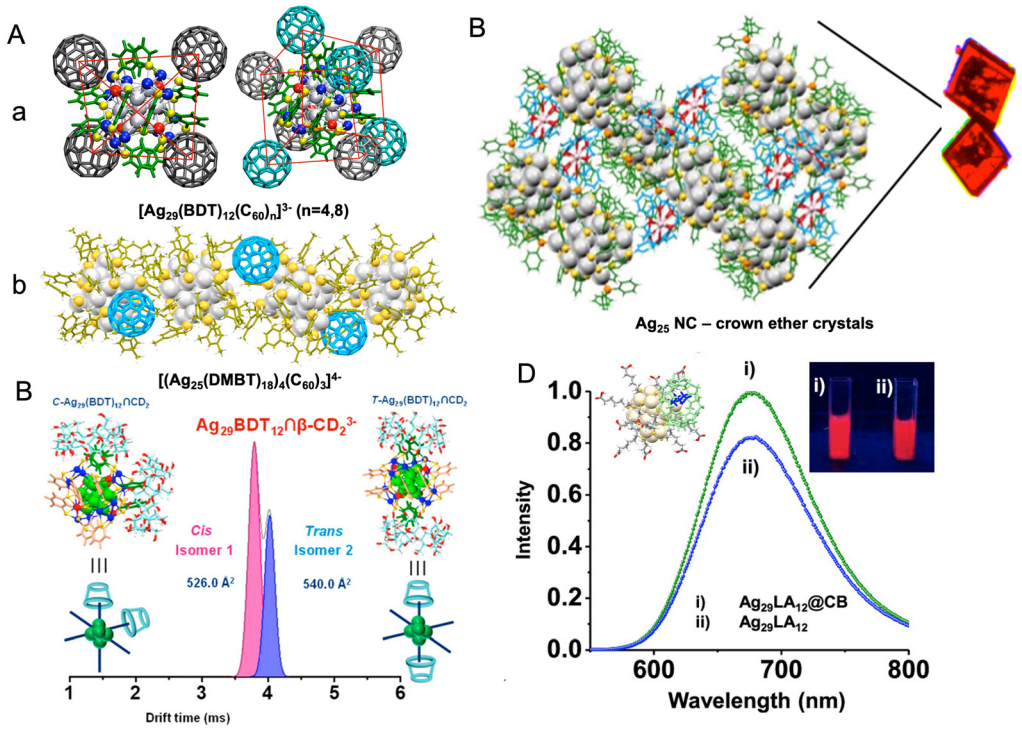

Fig. 9 (A) Host–guest complexes of (a) $Ag_{29}(BDT)_{12}^{3-}$ and (b) $Ag_{25}(DMBT)_{18}^-$ nanocluster with C_{60}, (B) crystal packing of $Ag_{29}(BDT)_{12}(TPP)_4^{3-}$ nanocluster with 18-crown-6-ether, (C) separation of isomers of the inclusion complex, $[Ag_{29}(BDT)_{12}(\beta\text{-CD})_2]^{3-}$ by ion mobility mass spectrometry, (D) enhancement in emission of $Ag_{29}LA_{12}$@CB complexes compared with that of $Ag_{29}LA_{12}$ nanocluster alone. Reproduced with permission from ref. A-a,[260] b,[261] B,[262] C,[263] and D.[264] Copyright 2018, 2019, and 2020 American Chemical Society.

gence of new properties in the host–guest complexes. Nag *et al.* reported inclusion complexes of $Ag_{29}(BDT)_{12}^{3-}$ nanocluster with CDs.[263] Such complexes showed isomerism due to the different binding possibilities of CDs on the nanocluster surface, as presented in Fig. 9C. About six CD attachments to the nanocluster were observed and the geometry of the supramolecular adducts resulted in isomerism similar to the octahedral coordination complexes of metals. Water-soluble and red luminescent $Ag_{29}(LA)_{12}$ (LA is lipoic acid) nanocluster also formed host–guest complexes with cucurbiturils and CDs which resulted in an enhancement in luminescence of the nanoclusters, as shown in Fig. 9D.[264] Such luminescent complexes were used for dopamine sensing. Pillar[5]arene-protected nanoclusters, $Ag_{29}(LA–P5)_{12}(TPP)_2$, were reported by Muhammed *et al.* which formed spherical assemblies with enhanced luminescence.[265] The reactivity of the nanoclusters was also reflected in their interaction with nanostructures like Au nanorods and Te nanorods to form a variety of self-assembled hybrid nanostructures (to be discussed later in detail). Recently, Sheng *et al.* reported the first supramolecular polymorphs of high-nuclearity Ag_{48} NCs encapsulated in an anionic template *via* solvent mediation.[266]

3.5 Intercluster reactions

Nanoclusters that undergo chemical reactions with one another, also known as intercluster reactions, are a rapidly developing field in nanoscience. Intercluster reactions are now utilized as tools to generate novel hybrid nanoclusters. It is crucial to have an atomic-level understanding of the chemical transformations of nanoclusters in such reactions. In this section, we will be discussing a few such examples of intercluster reactions and their associated mechanisms.

3.5.1. Diversity of reactions. In 2016, Krishnadas *et al.* reported the reaction between structurally and compositionally different $Au_{25}(PET)_{18}$ and $Ag_{44}(FTP)_{30}$ nanoclusters.[54] The intercluster reactions proceed through multiple intersystem exchanges involving both the metal and ligand to form alloy nanoclusters as the reaction product. The ESI mass spectra of the $Au_{25}(PET)_{18}$ and $Ag_{44}(FTP)_{30}$, and the reaction products, are shown in Fig. 10A. The mass spectrum shows a series of intercluster reaction products, like alloy nanoclusters formed from $Au_{25}(PET)_{18}$ by exchange of metal atoms (Au–Ag exchange), ligands (PET-FTP exchange) and metal–ligand fragments (Au-PET with Ag-FTP exchange). Similarly, the Au atoms, PET ligands and Au-PET fragments are also exchanged with $Ag_{44}(FTP)_{30}$, resulting in the formation of Ag-rich alloy nanoclusters. The total number of metal atoms, ligands, the overall structural features and the charge states of the nanoclusters are preserved in this reaction. Intercluster reaction was then studied for two structurally and compositionally analogous nanoclusters, $Au_{25}(PET)_{18}$ and $Ag_{25}(DMBT)_{18}$.[55] In this case, both interacting nanoclusters possess common structural features, like M_{13} (Ag/Au) icosahedral core and $M_2(SR)_3$ staple motifs. As shown in Fig. 10B, the ESI mass spectra of these two nanoclusters and the alloy nanoclusters formed as a reaction product were observed. Similarly, these nanoclusters also

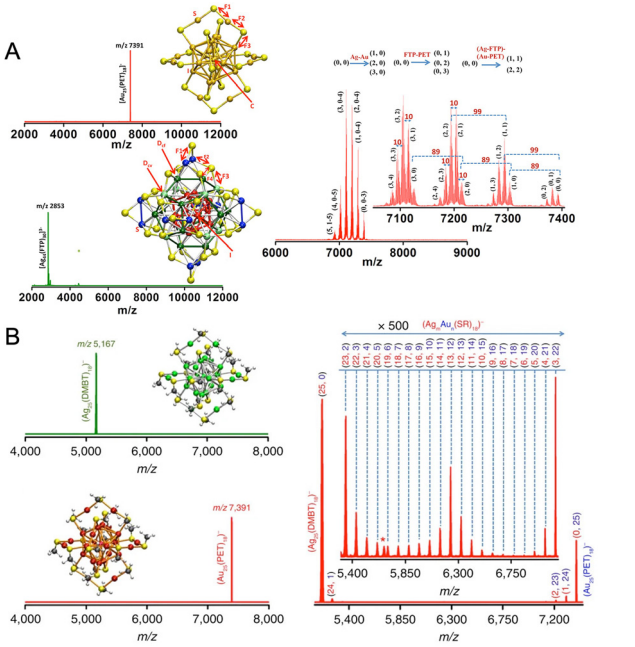

Fig. 10 Intercluster reaction of structurally and compositionally (A) different, $Au_{25}(PET)_{18}$ and $Ag_{44}(FTP)_{30}$, and (B) analogous $Au_{25}(PET)_{18}$ and $Ag_{25}(DMBT)_{18}$ nanoclusters. Adapted from ref. A,[54] and B.[55] Copyright 2016 American Chemical Society and Springer Nature Group.

exchange their metal atoms, ligands and metal–ligand fragments (Au-PET with Ag-DMBT exchange) to form alloy nanoclusters. Unlike the previous example, metal exchange (Ag–Au exchange) was only detected, and other exchanges, such as ligand (PET-DMBT exchange) and metal–ligand fragment (PET-DMBT exchange) were not detected in mass spectral measurements as the molecular masses of PET and DMBT ligands are equal. The mass spectrum collected after 2 min of reaction shows an entire range of alloy nanoclusters of $M_{25}(SR)_{18}$ composition as formed in the solution. Also, most importantly, in the course of reaction, the overall structure and charge of the nanocluster are conserved.

Several questions arise, such as (i) how two negatively charged nanoclusters interact despite the electrostatic repulsion and steric hindrance offered by the ligands, (ii) whether the reaction is driven by the entire nanocluster entity or any metal–thiolate fragments, and (iii) whether the reaction involves any intermediate or adduct species. In the next section, we will be discussing answers to a few of the questions, while a few remain unanswered.

3.5.2. Mechanism of intercluster reactions. To address the dynamics involved in the intercluster reactions in terms of atomic events, a systematic structural model is needed. Recent experiments suggest that the origin of any intercluster reactivity is the dynamic structure of nanoclusters in the solution. Of all the reported models, the Borromean ring model or *aspicule* (Greek meaning of "aspis" is the *shield*, with "molecule") model, wherein these nanoclusters are viewed as interlocked rings of metal thiolates (Fig. 11A), explains the intercluster

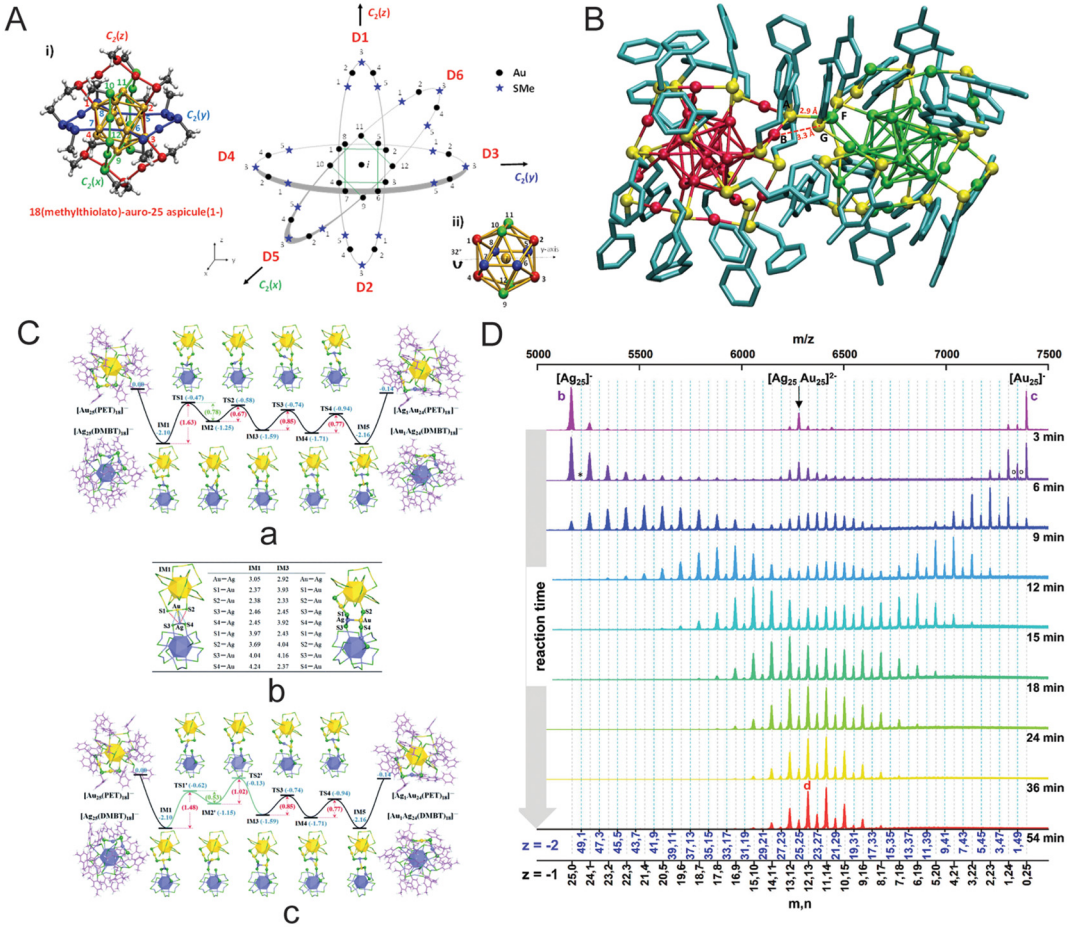

Fig. 11 (A) Borromean rings diagram of $Au_{25}(SMe)_{18}$, (B) DFT-optimization of the structure of $[Ag_{25}Au_{25}(DMBT)_{18}(PET)_{18}]^{2-}$ adduct (with Ag_{25} on the left and Au_{25} on the right) as obtained from a force-field-based molecular docking simulation, (C) energy profiles of the metal exchange reaction between the $[Au_{25}(PET)_{18}]^-$ and $[Ag_{25}(DMBT)_{18}]^-$ nanoclusters; (a) path 1 initiated by Au–S_{PET} bond breaking, (b) DFT optimized metal–metal and metal–S bond lengths (in Angstrom) (c) path 2 initiated by Ag–SDMBT bond breaking, and (D) time-dependent mass spectra of a 1 : 1 mixture of $[Au_{25}(PET)_{18}]^-$ and $[Ag_{25}(DMBT)_{18}]^-$. Reproduced with permissions from ref. A–B,[166] C,[270] and D.[271] Copyright 2015 and 2021 American Chemical Society. Copyright 2016, The Royal Chemical Society.

reaction better.[166] As per this model, an $M_{25}(SR)_{18}$ (M = Ag/Au) is composed of three interlocked $M_8(SR)_6$ rings around the central metal atom, M, where, the $M_{25}(SR)_{18}$ can be represented as $M@[M_8(SR)_6]_3$. The most important aspect of this *aspicule* model lies in the fact that the metal atoms (excluding the central metal) belong to a single structural unit, that is, metal-thiolate oligomeric rings, contrary to the *divide and protect* model, where the metal atoms belong to two distinct structural units, namely the innermost M_{13} icosahedron and the six outer $M_2(SR)_3$ staple units. The Borromean ring construction of the nanocluster suggests that in the event of metal–sulfur bond cleavage from any of the rings, the nanocluster can be reorganised as the entire cluster can be separated. This makes it possible for rapid metal exchange, as observed experimentally. In short, the Borromean ring model addresses the intercluster reactions in terms of the structural dynamics of the interlocked rings.

To study the mechanism of intercluster reactions, one needs to understand the role played by the metal–ligand interface in such reactions. The intercluster reaction is a redox-like reaction triggered by the difference in oxidation states of the metal atoms present in the core and staple. For example, let us consider the intercluster reaction between $Ag_{25}(SR)_{18}$ and $Au_{25}(SR)_{18}$.[55] Here, an $Ag_{25}(SR)_{18}$ molecule reacts with the $Au_2(SR)_3$ staples of $Au_{25}(SR)_{18}$, wherein Au in the $Au_2(SR)_3$ staples is in the +1 oxidation state. Similarly, an $Au_{25}(SR)_{18}$ molecule reacts with the $Ag_2(SR)_3$ staples of $Ag_{25}(SR)_{18}$, wherein Ag from the $Ag_2(SR)_3$ staple is in the +1 oxidation state. Such redox reactions between $M_{25}(SR)_{18}$ and M(I) thiolates, where M = Ag/Au, are well studied,[267,268] although it is still unclear how this difference in oxidation states contributes to the chemical reaction. Next, the intercluster reaction was studied for two entirely different nanoclusters, $Au_{25}(SR)_{18}$ and $Ag_{44}(SR)_{30}$, that resulted in the formation of reactive fragments like $Ag(SR)_2^-$, which further reacts with the $Au_2(SR)_3$ staples of $Au_{25}(SR)_{18}$, resulting in an exchange of metal atoms, ligands, and metal–ligand fragments.[54] In conclusion, the stability and chemical reactivity of these nanoclusters are characteristics of

the nature of the ligand and the bonding present in the metal–ligand oligomeric units.[58]

New insights into the intercluster reactions of $Au_{25}(PET)_{18}$ and $Ag_{25}(DMBT)_{18}$ came up with the detection of $[Ag_{25}Au_{25}(DMBT)_{18}(PET)_{18}]^{2-}$ adduct species.[55] Detection of such species indicates a possible pathway involving the formation of an adduct intermediate when two intact nanoclusters participate in these 'bimolecular' reactions. Using density functional theory (DFT), the Ag–S bond between the staples of the nanoclusters is observed in an optimized adduct structure (Fig. 11B). Computational studies suggest an interaction at the metal–ligand interface for the reacting nanoclusters at the early stages of the reaction. Furthermore, no metallic exchange was detected when nanoclusters, $Ag_xAu_{38-x}(SR)_{24}$ and $Au_{38}(SR)_{24}$, were separated by a dialysis membrane, and that suggests an intercluster collision as the origin of such reactions.[269]

In this section, some more mechanistic insights into the intercluster reactions are presented. More studies are needed to understand how two negatively charged nanoclusters collide, overcoming the electrostatic repulsion. One possible explanation for this could be coming from the fact that the anionic nanoclusters are not point charges; the overall negative charge is diffused over the entire nanocluster entity. At the early stages of the reaction, the intercluster interaction could lead to collisions, electron transfer, *etc.*, resulting in nanocluster destabilization. The destabilization of the nanocluster eventually may lead to ring opening (refer to the Borromean ring model) followed by it taking up a flexible elongated conformation, allowing atoms to interact freely with other nanoclusters. At this stage, the nanoclusters with open rings can interact more easily and undergo metal, ligand, and metal–ligand fragment exchanges. The Borromean ring model of $Au_{25}(SR)_{18}$ suggests the spontaneous inclusion of Ag-atom in the nanocluster core as it is not sterically hindered. Theoretical calculations were performed by Huang *et al.* to understand the intercluster exchange reaction mechanism between $Au_{25}(SR)_{18}$ and $Ag_{25}(SR)_{18}$ (Fig. 11C).[270] As per calculations, the intercluster reactions are a two-step mechanism: (i) dianionic adduct $[Au_{25}Ag_{25}(PET)_{18}(DMBT)_{18}]^{2-}$ intermediate formation followed by metal–ligand staple rearranges to facilitate metal exchange, and (ii) then the heterometal atom in the staple swaps with the metal atom present in the icosahedral M_{13}-kernel. Recently, Neumaier *et al.* reported a detailed experimental and computational study of the intercluster reaction kinetics of $Au_{25}(PET)_{18}$ and $Ag_{25}(DMBT)_{18}$ at room temperature.[271] During the reaction, the participation of both nanocluster monomer and dimers were observed in mass spectral and collision-induced dissociation (CID) measurements. For an equimolar concentration of nanoclusters, time-dependent mass spectra show a sufficient abundance of both monomers and dimers along with continuous change in overall Ag : Au compositions until a dynamic equilibrium is achieved (Fig. 11D). The kinetic model suggested a three-step reaction route involving dimerization of monomers, metal atom exchange in the transient dimer, and dimer dissociation.

Chakraborty *et al.* reported isotopic metal exchanges in nanoclusters, which provided further insights into the mechanism of atom transfer in NPs. Two isotopic $Ag_{25}(DMBT)_{18}^-$ nanoclusters, made from ^{107}Ag and ^{109}Ag, reacted spontaneously in solution to form an isotopically mixed nanocluster (Fig. 12A).[272] Such isotopic exchanges were similar to isotopic exchanges in H_2O/D_2O, further supporting the molecular nature of the nanoclusters. The exchange was rapid and occurred within seconds after mixing the solutions at room temperature. The exchange could be controlled by controlling the temperature. The exchange kinetics was better studied

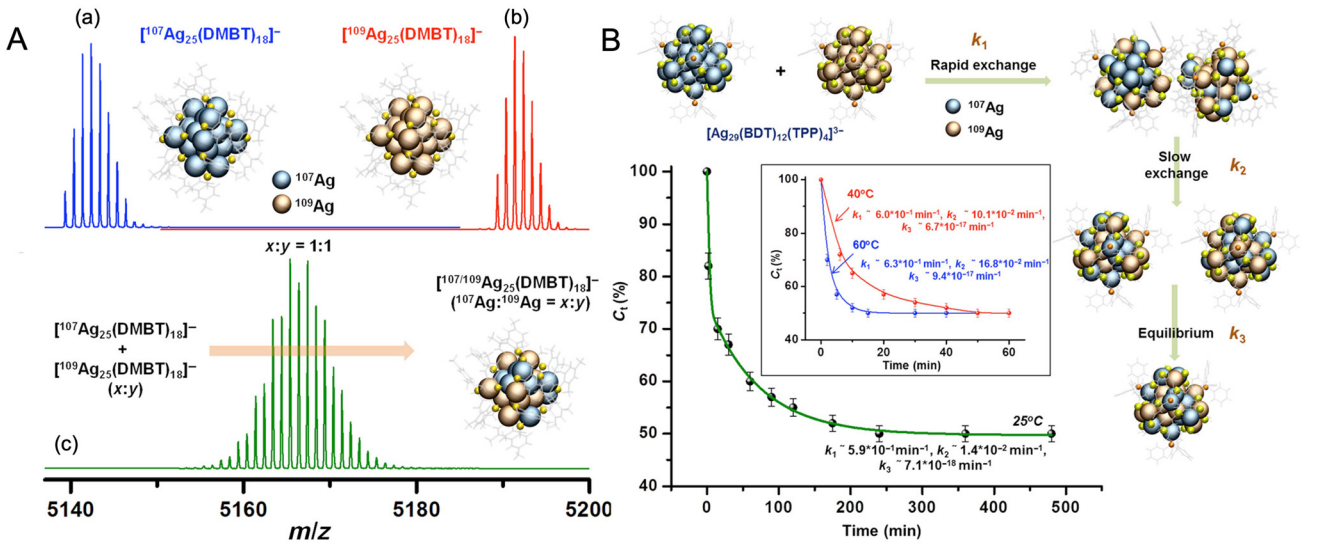

Fig. 12 (A) ESI MS of (a) $[^{107}Ag_{25}(DMBT)_{18}]^-$, (b) $[^{109}Ag_{25}(DMBT)_{18}]^-$, and (c) isotopically mixed $[Ag_{25}(DMBT)_{18}]^-$ nanocluster with $^{107}Ag : {}^{109}Ag$ ratio of 1 : 1. (B) Kinetics of isotopic Ag atom exchange in $[Ag_{29}(BDT)_{12}(TPP)_4]^{3-}$ nanocluster. Adapted from ref. 272. Copyright 2019 American Association for the Advancement of Science.

using a more rigid nanocluster system, $Ag_{29}(BDT)_{12}(TPP)_4^{3-}$, which exhibited slower exchange rates. Similar isotopic $^{107}Ag/^{109}Ag$ atom exchange was also observed in this case, and a time-resolved study revealed that the process involved an initial fast reaction rate, probably arising from atom exchanges in the staples, followed by a slow reaction rate arising from the diffusion of atoms from staple to core and a final state where the exchanged atoms rearrange until they attain the thermodynamic equilibrium state (Fig. 12B). Such an exchange process was driven by the entropy of mixing. These results suggested the dynamic nature of the metal atom transfer in nanoclusters in solution. The dynamic nature of the ligand monolayers was also reported in a study by Salassa *et al.*[273] The metal–ligand interface also plays an important role in controlling atom transfer and intercluster reactions of nanoclusters.

3.6. Interparticle reactions: reactions with higher dimension materials

In 2014, Ghosh *et al.* made the first attempt to study the chemical interactions between atomically precise nanoclusters with other nanomaterials.[274] In this study, graphene reacted with $Au_{25}(PET)_{18}$, resulting in the formation of a larger nanocluster, $Au_{135}(PET)_{57}$. The conversion of $Au_{25}(PET)_{18}$ nanocluster was monitored using time-dependent matrix-assisted laser desorption ionization mass spectrometry (MALDI MS) (Fig. 13A). As the reaction progressed, the nanocluster peak at *m/z* 7391 due to $Au_{25}(PET)_{18}$ gradually disappeared with the simultaneous evolution of the peak at *m/z* 34.4 kDa corresponding to $Au_{135}(PET)_{57}$. This conversion process is driven by an overall energy gain of the system due to the entrapment of smaller nanoclusters at the local valleys of the graphenic surface resulting in the reduction in surface curvature and, finally, leading to coalescence. This study gave insights into the utility of surface as a reactive substrate for the chemical transformations of ligand-protected metal nanoclusters.

Unique reactivity of water-soluble $Au_{32}SG_{19}$ nanocluster to Te nanowires (NWs) was reported by Som *et al.*[275] This reaction results in the formation Ag–Te hybrid NWs with the growth of nodule-shaped Ag NPs on the NW surface (Fig. 13B). Structural analysis of the modified Te NWs using HRTEM-EDS and XRD confirmed the presence of Ag as nodules with Te NW retaining its inherent (001) hexagonal structure. Furthermore, on heating the Ag-decorated Te NWs, the morphology evolves into nano dumbbell-shaped Ag–Te–Ag NWs with Ag NPs specifically located at the tips (Fig. 13B). The ultrasmall size of the $Ag_{32}SG_{19}$ nanocluster provides an increased surface free energy, thereby inducing a tendency of intercluster coalescence, resulting in bigger particles.

Ligand-protected metal nanoclusters make excellent building blocks to create self-assembled hierarchical frameworks.[192,276,277] An interesting phenomenon of self-assembly arises in Te NWs when the surface is modified with $Ag_{44}(p\text{-MBA})_{30}$ nanocluster. The *p*-MBA ligand shells initiate a H-bonding interaction among themselves, leading to the formation of a bilayer assembly of NWs oriented at an angle of 81° w.r.t. each other (Fig. 14A).[278] Nonappa *et al.* reported the

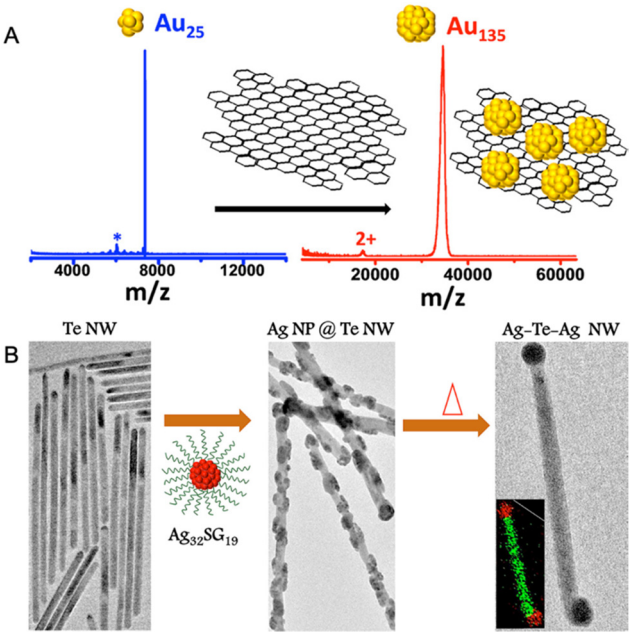

Fig. 13 (A) MALDI MS study for the conversion of $Au_{25}(PET)_{18}$ to $Au_{135}(PET)_{57}$ entrapped on the on the graphene surface upon reaction with graphene. (B) HRTEM images and corresponding schematic representation of pure Te NW upon reaction with $Ag_{32}SG_{19}$ and upon further heating yielding Ag nodule-decorated Te NW and dumbbell-shaped Ag–Te–Ag NWs, respectively. Adapted from ref. 274 and 275 for A and B, respectively. Copyright 2014 American Chemical Society.

unique ability of *p*-MBA-protected gold nanoclusters to undergo intercluster H-bonding resulting in monolayer-thick 2D nanosheets and spherical capsids.[276,279] Som *et al.* showed that the Na_4Ag_{44}-*p*MBA_{30} nanoclusters can be self-assembled into a large-area freestanding elastic membrane *via* entrapping them in a transient solvent layer at the air–water interface.[280] The patchy distribution of ligands around the metal core facilitates symmetry breaking and eventually directs a preferential interlayer H-bonding between the carboxylic acid groups of the *p*-MBA ligands.[276,277,279] Chakraborty *et al.* showed hydrogen bonding-induced chemical interaction between the $Ag_{44}(p\text{-MBA})_{30}$ nanocluster and a plasmonic gold nanorod (GNR), leading to the encapsulation of the latter (Fig. 14B), here denoted as GNR@Ag_{44}.[281] The nanocage-like hybrid material was found to have an octahedral morphology as studied using a series of highly sophisticated microscopes, like transmission electron microscopy (TEM), scanning transmission electron microscopy (STEM), and 3D reconstruction using electron tomography. The anisotropic growth was credited to the preferential anchoring of the nanoclusters to Au ⟨110⟩ over Au ⟨100⟩ facet of GNR@*p*-MBA. $Ag_{25}(DMBT)_{18}$ nanocluster-mediated site-selective etching of anisotropic planar gold nanotriangles (NTs) was reported.[282] Due to differential surface energies, the Au NTs interacting with the nanocluster underwent metallic etching at the edges and doping at the tips while the core remained unaltered. Roy *et al.* reported a polydispersed CuO NP and $Au_{25}(PET)_{18}$ reaction-mediated formation of spherical-

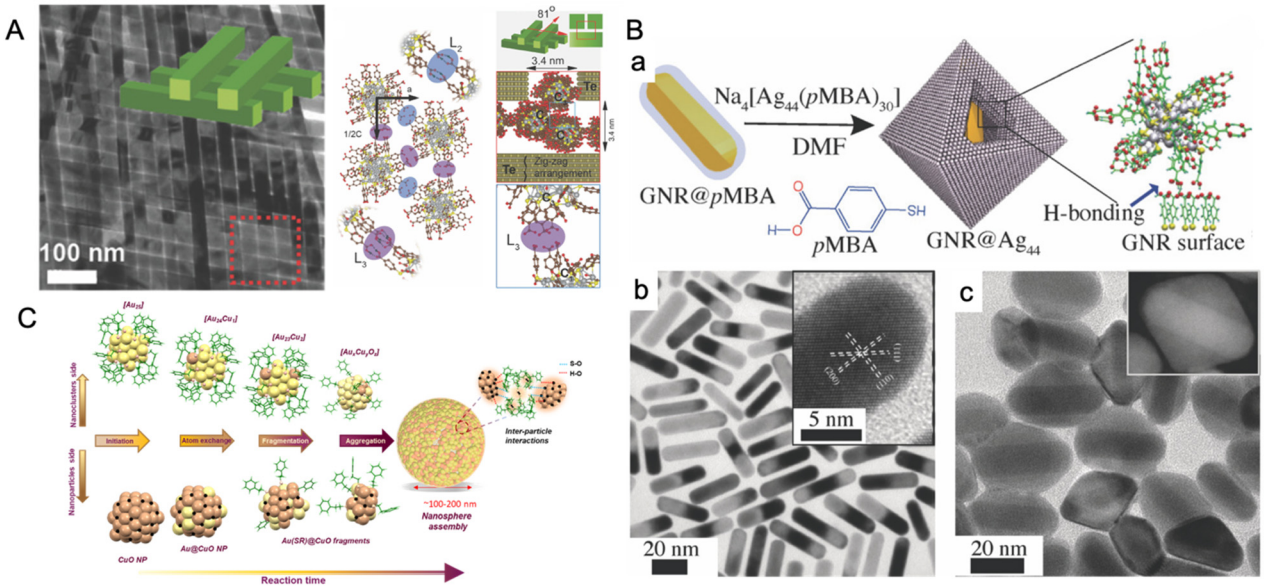

Fig. 14 (A) Composite Ag_{44}@Te NW bilayer oriented at an 81° angle w.r.t to each other and (B) its corresponding packing driven by the intercluster H-bonding. (C) Schematic representation and HRTEM micrographs illustrating the assembly of Ag_{44} on the GNR. Adapted from ref. A,[278] B,[281] and C.[283] Copyright 2014 and 2018, John Wiley and Sons. Copyright 2023, The Royal Society of Chemistry.

shaped nanoaggregates of Cu-doped-Au-nanoclusters (Fig. 14C).[283] The reaction involved an NP–NC atom transfer reaction route. Rival *et al.* recently demonstrated that the thiolated azobenzene-protected Au_{25} nanoclusters form reversible assemblies triggered by light.[284] With the right choice of nanocluster system, such hybrid nanomaterials having extraordinary stability at room temperature can significantly improve the limit of detection of nanocluster-based sensors.

Bose *et al.* extended the interparticle chemistry to the reactions involving isotropic Ag NPs.[285] A spontaneous reaction between $Au_{25}(PET)_{18}$ nanocluster and polydispersed Ag NPs with a core diameter of 4.4 ± 2.3 nm, protected with 2-phenylethanethiol (PET), resulted in monodispersed alloy NPs with a core diameter of 3.4 ± 1.2 nm under ambient conditions. The resulting NPs also underwent a spontaneous self-assembly to form a 2D superlattice which was analysed using HRTEM. Using STEM-EDS analysis, the reacted NPs were found to be Ag–Au alloy NPs. A 3D reconstruction of the 2D assembly using electron tomography further revealed that the assembly was composed of reacted alloy NPs arranged in a hexagonal close-packed (hcp) lattice with an interparticle distance of ~4.5 nm (Fig. 15A). The mechanism involved an interparticle

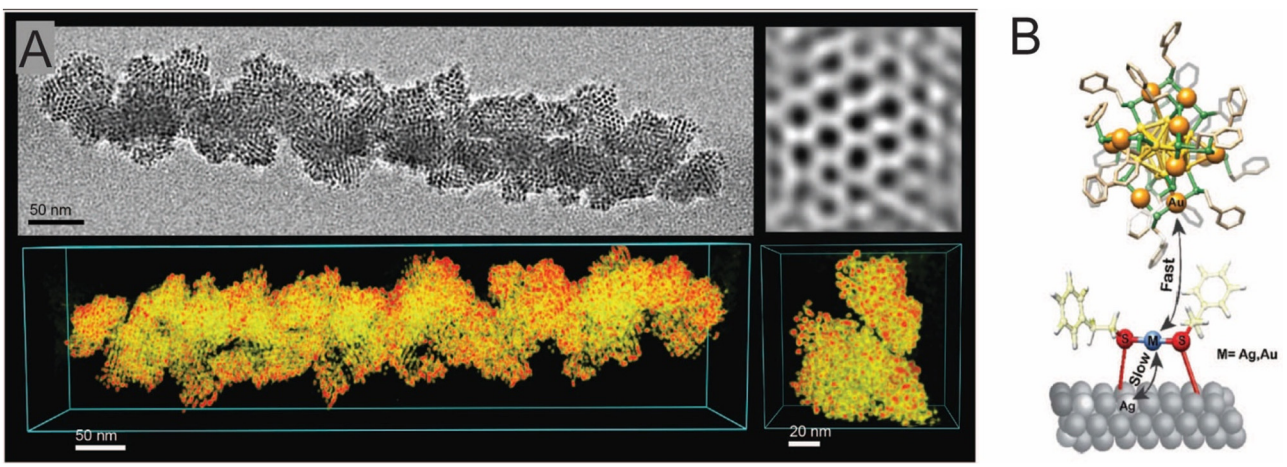

Fig. 15 (A) TEM micrograph, its corresponding 3D reconstruction, and inverse fast Fourier transform image of 2D superlattice assembly (hcp) of the Au–Ag alloy NP resulting from the NP–nanocluster reaction. (B)The number of Ag-doped Au nanocluster *versus* time plot for the nanocluster–Ag surface reaction and the schematic representation metallic exchange at the metal–ligand interface on the bulk surface. Reproduced with permission A[285] and B.[288] Copyright 2020 Royal Society of Chemistry. Copyright 2008 American Chemical Society.

atomic exchange (metal–ligand species), and the metal–ligand interface was found to be crucial in controlling the reaction. Systematic analysis using time-dependent ESI MS showed that the reaction proceeds through a transient $Au_{25-x}Ag_x(PET)_{18}$ (x = 1, 2, 3,...,) species along with other alloy nanocluster intermediates. Similar reactions were performed for $Au_{25}(PET)_{18}$ nanocluster with differently sized Ag@PET NPs, in which the interparticle reactivity was enhanced upon decreasing the size of NPs. The nanocluster–NP reactions can thereby open up an entirely new way of generating alloy NPs in the solution phase with better control over the NP size distribution.

As we move from noble metal nanosystems to their bulk counterparts, chemical properties are altered due to changes in energy levels. Baksi *et al.* explored the glucose-mediated extraction of Ag from bulk silver surfaces otherwise considered inert.[286] Later, Nag *et al.* reported the solution phase synthesis of Ag nanoclusters from bulk metallic silver in the presence of carbohydrate and glutathione followed by chemical reduction.[287] Kazan *et al.* utilized the bulk thiolated silver surface to understand intercluster reaction as an interfacial phenomenon of metal–ligand exchange.[288] The study involved $Au_{25}(PET)_{18}$ and $Au_{38}(PET)_{24}$ nanoclusters, and pure silver foil as model systems. MALDI MS and XPS characterization techniques were used to study the effect of reaction on the nanocluster and foil, respectively. Upon time-dependent monitoring of the $Au_{25}(PET)_{18}$ and PET-monolayered Ag foil, $Au_{25-x}Ag_x(PET)_{18}$ (x = 1–4) appeared just after 2 min and a higher Ag-doping was detected for a longer reaction time. With the neat Ag foil, the reaction was found to be slow, as $Au_{24}Ag(PET)_{18}$ appeared only after 3 h. Hence, the kinetics of pre-adsorbed and neat silver foils are very different. The average number of doped Ag plotted as a function of time shows that the substitution follows a 2-phase kinetics (initially fast followed by slower exchange) and a sigmoidal trend (initially delayed followed by faster exchange) in preadsorbed and neat foils, respectively. This sigmoidal kinetics can be related to the autocatalytic reactions where the starting 3 h is an induction period for the thiolate, here acting as a catalyst, to deposit on the surface. As the time progressed, thiolate deposition happened, and this is reflected with an increased reaction rate. The mechanism behind the 2-phase kinetics in an atomic exchange reaction was explained using the scheme in which thiolated-Ag on the surface exchanges faster in the early stages of the reaction (Fig. 15B). At the later stages of the reaction, kinetics become slower due to less availability of exchangeable sites on the Ag foil surface. XPS measurements of the reacted Ag foil surface showed the presence of the metallic Au. Similar trends were observed when the $Au_{38}(PET)_{18}$ nanocluster reacts with both the pre-adsorbed and neat Ag surfaces. XPS measurements of the reacted pre-adsorbed thiolated and neat foils also confirmed the presence of metallic Au. The $Au_{25}(PET)_{18}$ and $Au_{38}(PET)_{18}$ reaction was also explored with pre-adsorbed and free surface of other metals like Cd and Cu. This study concluded that for a feasible Au doping in the Ag nanocluster, thiol plays a key role. Recently, Chakraborty *et al.* reported the dynamics of isotopic exchange reactions of isotopically pure Ag nanocluster with different dimensions of metallic Ag, like nanoclusters, plasmonic NPs, and bulk.[289] Isotopically pure $^{107}Ag_{25}(DMBT)_{18}$ and $^{108}Ag_{25}(DMBT)_{18}$ was reacted with different sizes of Ag@DMBT NPs (naturally abundant Ag). With the increase in the NP size, the rate of atomic exchange was reduced. The exchange rate further decreased when the nanocluster was reacted with bulk Ag samples, such as foil and micron-sized powder. The kinetics of isotopic exchange, *i.e.*, reaction timescales, was analyzed by fitting the reactant concentration as a function of time to a reaction model. Under similar reaction conditions, the reaction timescale was longer for the nanocluster-NP reactions compared with intercluster reactions. This suggests that suchreactions can be controlled by careful engineering the reacting nanostructures.

4. Insights from nanocluster chemistry

From the results presented, we list below the factors determining the feasibility of reactions of nanoclusters.

(1) The metal–ligand interface primarily controls the atomic exchange reactions and their feasibility.

(2) The geometry and stereochemistry of the protecting groups play crucial roles in the intercluster and interparticle reactions.

(3) Thermodynamics drives the interparticle and isotopic exchange reactions.

(4) Entropy of mixing drives the isotopic metal exchange in intercluster reactions.

(5) Nanoclusters exhibit redox-like reactions triggered by the difference in oxidation states of the metal atoms present in the core and staple.

(6) The core–shell geometry of a nanocluster influences the nanocluster–analyte reaction primarily *via* weak interactions, such as metallophilic and supramolecular interactions.

(7) Supramolecular interactions like C–H···π, π···π, van der Waals, hydrogen bonding, and electrostatic interactions guide the formation of the nanocluster assemblies.

(8) Reactive intermediates, such as adducts and fragments, vary depending on the reacting species.

(9) LEIST, a method to prepare new nanoclusters, is a ligand-controlled phenomenon. The rate of ligand exchange depends also on the electron-donating or withdrawing nature of the ligand.

(10) Chemical reactions occur between atomically precise nanoclusters and a range of systems such as ions, clusters, NPs, and bulk metals, and therefore we may suggest that nanoclusters are reactive to the whole range of chemical systems.

(11) The chemistry is highly sensitive to reaction conditions such as concentration, time, and temperature, and is expected to be influenced by other factors such as the medium, ionic strength, *etc.*

5. Conclusions and future perspectives

Nanoclusters, with their inherent molecule-like properties, show a wide range of chemical reactions with counterparts such as metal ions, clusters, NPs and bulk metals. These chemical reactions yield well-defined alloys which may be nanoclusters, NPs or bulk materials, depending on the systems involved. Such reactions also lead to ligand exchange. The processes yield supramolecular interactions forming assemblies and superstructures. Thermodynamics and kinetics govern the chemistry, and the underlying processes can be modelled with greater accuracy. The chemistry is sensitive to various process conditions such as concentration, temperature, solvent, *etc.*, as typical of molecular events. The products formed and their kinetics and dynamics confirm their molecular nature. In the coming years, such cluster chemistry of atomically precise metal nanoclusters will be explored with oxides, sulfides, and others in the form of clusters, NPs, and bulk materials, yielding new materials. Similar science will be possible between materials of different size regimes of oxides and sulfides themselves, expanding the diversity of the area. The science presented will be greatly influenced by the experimental and computational methodologies used, which can reveal the intricate details of the processes involved. The science at this stage has provided us with many insights into the phenomena at the nanoscale as revealed by the fast isotopic exchange between NPs. Applications of such science are still at infancy.

Author contributions

All authors contributed equally.

Conflicts of interest

There are no conflicts to declare.

Acknowledgements

We acknowledge the Department of Science and Technology (DST), Government of India, and Centre of Excellence program of the Indian Institute of Technology Madras, on the theme of Molecular Materials and Functions, under the Institutions of Eminence of Ministry of Education, India, for supporting our research.

References

1 R. Feynman, *Feynman And Computation*, CRC Press, 2002.
2 F. A. Cotton and J. T. Mague, *Inorg. Chem.*, 1964, **3**, 1094–1098.
3 F. A. Cotton, *Inorg. Chem.*, 1964, **3**, 1217–1220.
4 R. W. Murray, *Chem. Rev.*, 2008, **108**, 2688–2720.
5 G. Chen, J. Seo, C. Yang and P. N. Prasad, *Chem. Soc. Rev.*, 2013, **42**, 8304–8338.
6 H. Zhu, Y. Yang and T. Lian, *Acc. Chem. Res.*, 2013, **46**, 1270–1279.
7 R. Jin, C. Zeng, M. Zhou and Y. Chen, *Chem. Rev.*, 2016, **116**, 10346–10413.
8 Y. Du, H. Sheng, D. Astruc and M. Zhu, *Chem. Rev.*, 2020, **120**, 526–622.
9 T. Tsukuda and H. Hakkinen, *Protected Metal Clusters: From Fundamentals to Applications*, 2013, vol. 53.
10 A. Ghosh, O. F. Mohammed and O. M. Bakr, *Acc. Chem. Res.*, 2018, **51**, 3094–3103.
11 I. Chakraborty and T. Pradeep, *Chem. Rev.*, 2017, **117**, 8208–8271.
12 R. Jin, *Nanoscale*, 2010, **2**, 343–362.
13 V. G. Albano, P. L. Bellon, M. Manassero and M. Sansoni, *J. Chem. Soc. D*, 1970, 1210–1211.
14 C. E. Briant, B. R. C. Theobald, J. W. White, L. K. Bell, D. M. P. Mingos and A. J. Welch, *J. Chem. Soc., Chem. Commun.*, 1981, 201–202.
15 *Atomically precise metal clusters*, ed. T. Pradeep, Elsevier, 1st edn, 2023.
16 S. S. Narayanan and S. K. Pal, *J. Phys. Chem. C*, 2008, **112**, 4874–4879.
17 J. Xie, Y. Zheng and J. Y. Ying, *J. Am. Chem. Soc.*, 2009, **131**, 888–889.
18 J. Yu, S. Choi and R. M. Dickson, *Angew. Chem., Int. Ed.*, 2009, **48**, 318–320.
19 P. L. Xavier, K. Chaudhari, A. Baksi and T. Pradeep, *Nano Rev.*, 2012, **3**, 14767.
20 X. Wen, P. Yu, Y. R. Toh, A. C. Hsu, Y. C. Lee and J. Tang, *J. Phys. Chem. C*, 2012, **116**, 19032–19038.
21 D. M. Chevrier, V. D. Thanthirige, Z. Luo, S. Driscoll, P. Cho, M. A. MacDonald, Q. Yao, R. Guda, J. Xie, E. R. Johnson, A. Chatt, N. Zheng and P. Zhang, *Chem. Sci.*, 2018, **9**, 2782–2790.
22 T. Vosch, Y. Antoku, J. C. Hsiang, C. I. Richards, J. I. Gonzalez and R. M. Dickson, *Proc. Natl. Acad. Sci. U. S. A.*, 2007, **104**, 12616–12621.
23 H. C. Yeh, J. Sharma, J. J. Han, J. S. Martinez and J. H. Werner, *Nano Lett.*, 2010, **10**, 3106–3110.
24 J. T. Petty, B. Sengupta, S. P. Story and N. N. Degtyareva, *Anal. Chem.*, 2011, **83**, 5957–5964.
25 J. Sharma, H. C. Yeh, H. Yoo, J. H. Werner and J. S. Martinez, *Chem. Commun.*, 2011, **47**, 2294–2296.
26 E. Gwinn, D. Schultz, S. M. Copp and S. Swasey, *Nanomaterials*, 2015, **5**, 180–207.
27 D. J. E. Huard, A. Demissie, D. Kim, D. Lewis, R. M. Dickson, J. T. Petty and R. L. Lieberman, *J. Am. Chem. Soc.*, 2019, **141**, 11465–11470.
28 L. A. Peyser, A. E. Vinson, A. P. Bartko and R. M. Dickson, *Science*, 2001, **291**, 103–106.
29 L. A. Peyser, T. H. Lee and R. M. Dickson, *J. Phys. Chem. B*, 2002, **106**, 7725–7728.

30 J. Zheng and R. M. Dickson, *J. Am. Chem. Soc.*, 2002, **124**, 13982–13983.
31 J. Zheng, C. Zhang and R. M. Dickson, *Phys. Rev. Lett.*, 2004, **93**, 077402, 8AD.
32 M. C. Paau, C. K. Lo, X. Yang and M. M. F. Choi, *J. Phys. Chem. C*, 2010, **114**, 15995–16003.
33 E. S. Shibu and T. Pradeep, *Chem. Mater.*, 2011, **23**, 989–999.
34 A. George, E. S. Shibu, S. M. Maliyekkal, M. S. Bootharaju and T. Pradeep, *ACS Appl. Mater. Interfaces*, 2012, **4**, 639–644.
35 M. Mayer, M. Rohdenburg, V. van Lessen, M. C. Nierstenhöfer, E. Aprà, S. Grabowsky, K. R. Asmis, C. Jenne and J. Warneke, *Chem. Commun.*, 2020, **56**, 4591–4594.
36 H. W. Kroto, J. R. Heath, S. C. O'Brien, R. F. Curl and R. E. Smalley, *Nature*, 1985, **318**, 162–163.
37 H. W. Kroto, A. W. Allaf and S. P. Balm, *Chem. Rev.*, 1991, **91**, 1213–1235.
38 J. Almutlaq, J. Yin, O. F. Mohammed and O. M. Bakr, *J. Phys. Chem. Lett.*, 2018, **9**, 4131–4138.
39 Y. Yan, J. Gong, J. Chen, Z. Zeng, W. Huang, K. Pu, J. Liu and P. Chen, *Adv. Mater.*, 2019, **31**, 1808283.
40 R. B. Wyrwas, M. M. Alvarez, J. T. Khoury, R. C. Price, T. G. Schaaff and R. L. Whetten, *Eur. Phys. J. D*, 2007, **43**, 91–95.
41 H. Häkkinen, *Chem. Soc. Rev.*, 2008, **37**, 1847–1859.
42 Y. Negishi, T. Iwai and M. Ide, *Chem. Commun.*, 2010, **46**, 4713–4715.
43 C. M. Aikens, *J. Phys. Chem. Lett.*, 2011, **2**, 99–104.
44 O. Lopez-Acevedo, H. Tsunoyama, T. Tsukuda, H. Häkkinen and C. M. Aikens, *J. Am. Chem. Soc.*, 2010, **132**, 8210–8218.
45 R. Jin, *Nanoscale*, 2015, **7**, 1549–1565.
46 C. M. Aikens, *Acc. Chem. Res.*, 2018, **51**, 3065–3073.
47 Q. Tang, G. Hu, V. Fung and D. Jiang, *Acc. Chem. Res.*, 2018, **51**, 2793–2802.
48 R. S. Ingram, M. J. Hostetler, R. W. Murray, T. G. Schaaff, J. T. Khoury, R. L. Whetten, T. P. Bigioni, D. K. Guthrie and P. N. First, *J. Am. Chem. Soc.*, 1997, **119**, 9279–9280.
49 D. Lee, R. L. Donkers, J. M. DeSimone and R. W. Murray, *J. Am. Chem. Soc.*, 2003, **125**, 1182–1183.
50 M. Zhu, C. M. Aikens, F. J. Hollander, G. C. Schatz and R. Jin, *J. Am. Chem. Soc.*, 2008, **130**, 5883–5885.
51 D. Jiang, M. L. Tiago, W. Luo and S. Dai, *J. Am. Chem. Soc.*, 2008, **130**, 2777–2779.
52 P. Yu, X. Wen, Y.-R. Toh, X. Ma and J. Tang, *Part. Part. Syst. Charact.*, 2015, **32**, 142–163.
53 S. Chen, R. S. Ingram, M. J. Hostetler, J. J. Pietron, R. W. Murray, T. G. Schaaff, J. T. Khoury, M. M. Alvarez and R. L. Whetten, *Science*, 1998, **280**, 2098–2101.
54 K. R. Krishnadas, A. Ghosh, A. Baksi, I. Chakraborty, G. Natarajan and T. Pradeep, *J. Am. Chem. Soc.*, 2016, **138**, 140–148.
55 K. R. Krishnadas, A. Baksi, A. Ghosh, G. Natarajan and T. Pradeep, *Nat. Commun.*, 2016, **7**, 13447.
56 K. R. Krishnadas, A. Baksi, A. Ghosh, G. Natarajan, A. Som and T. Pradeep, *Acc. Chem. Res.*, 2017, **50**, 1988–1996.
57 S. Hossain, Y. Niihori, L. V. Nair, B. Kumar, W. Kurashige and Y. Negishi, *Acc. Chem. Res.*, 2018, **51**, 3114–3124.
58 K. R. Krishnadas, G. Natarajan, A. Baksi, A. Ghosh, E. Khatun and T. Pradeep, *Langmuir*, 2019, **35**, 11243–11254.
59 T. Kawawaki, A. Ebina, Y. Hosokawa, S. Ozaki, D. Suzuki, S. Hossain and Y. Negishi, *Small*, 2021, **17**, 2005328.
60 N. Goswami, Q. Yao, Z. Luo, J. Li, T. Chen and J. Xie, *J. Phys. Chem. Lett.*, 2016, **7**, 962–975.
61 X. Kang and M. Zhu, *Chem. Soc. Rev.*, 2019, **48**, 2422–2457.
62 S. Biswas, A. K. Das and S. Mandal, *Acc. Chem. Res.*, 2023, **56**, 1838–1849.
63 Y. Xiao, Z. Wu, Q. Yao and J. Xie, *Aggregate*, 2021, **2**, 114–132.
64 Y. Negishi, H. Tsunoyama, M. Suzuki, N. Kawamura, M. M. Matsushita, K. Maruyama, T. Sugawara, T. Yokoyama and T. Tsukuda, *J. Am. Chem. Soc.*, 2006, **128**, 12034–12035.
65 M. Zhu, C. M. Aikens, M. P. Hendrich, R. Gupta, H. Qian, G. C. Schatz and R. Jin, *J. Am. Chem. Soc.*, 2009, **131**, 2490–2492.
66 S. Antonello, N. V. Perera, M. Ruzzi, J. A. Gascón and F. Maran, *J. Am. Chem. Soc.*, 2013, **135**, 15585–15594.
67 M. Agrachev, S. Antonello, T. Dainese, J. A. Gascón, F. Pan, K. Rissanen, M. Ruzzi, A. Venzo, A. Zoleo and F. Maran, *Chem. Sci.*, 2016, **7**, 6910–6918.
68 M. Agrachev, S. Antonello, T. Dainese, M. Ruzzi, A. Zoleo, E. Aprà, N. Govind, A. Fortunelli, L. Sementa and F. Maran, *ACS Omega*, 2017, **2**, 2607–2617.
69 M. Agrachev, M. Ruzzi, A. Venzo and F. Maran, *Acc. Chem. Res.*, 2019, **52**, 44–52.
70 M. Galchenko, A. Black, L. Heymann and C. Klinke, *Adv. Mater.*, 2019, **31**, 1–6.
71 P. Yuan, R. Zhang, E. Selenius, P. Ruan, Y. Yao, Y. Zhou, S. Malola, H. Häkkinen, B. K. Teo, Y. Cao and N. Zheng, *Nat. Commun.*, 2020, **11**, 2229.
72 G. Zhang, Y. Li, J. Xu, C. Zhang, S. Shuang, C. Dong and M. M. F. Choi, *Sens. Actuators, B*, 2013, **183**, 583–588.
73 X. Yuan, Y. Tay, X. Dou, Z. Luo, D. T. Leong and J. Xie, *Anal. Chem.*, 2013, **85**, 1913–1919.
74 X. Chen, J. B. Essner and G. A. Baker, *Nanoscale*, 2014, **6**, 9594–9598.
75 A. Mathew and T. Pradeep, *Part. Part. Syst. Charact.*, 2014, **31**, 1017–1053.
76 G. Schmid, *Chem. Soc. Rev.*, 2008, **37**, 1909–1930.
77 L. Shang, S. Dong and G. U. Nienhaus, *Nano Today*, 2011, **6**, 401–418.
78 S. Choi, R. M. Dickson and J. Yu, *Chem. Soc. Rev.*, 2012, **41**, 1867–1891.
79 X. R. Song, N. Goswami, H. H. Yang and J. Xie, *Analyst*, 2016, **141**, 3126–3140.
80 L. Zhang and E. Wang, *Nano Today*, 2014, **9**, 132–157.

81 S. Yamazoe, K. Koyasu and T. Tsukuda, *Acc. Chem. Res.*, 2014, **47**, 816–824.
82 P. Liu, R. Qin, G. Fu and N. Zheng, *J. Am. Chem. Soc.*, 2017, **139**, 2122–2131.
83 L. Liu and A. Corma, *Chem. Rev.*, 2018, **118**, 4981–5079.
84 W. Jing, H. Shen, R. Qin, Q. Wu, K. Liu and N. Zheng, *Chem. Rev.*, 2023, **123**, 5948–6002.
85 A. Henglein, *J. Phys. Chem.*, 1979, **83**, 2209–2216.
86 A. Henglein and R. Tausch-Treml, *J. Colloid Interface Sci.*, 1981, **80**, 84–93.
87 A. Henglein, *J. Phys. Chem.*, 1993, **97**, 5457–5471.
88 A. Henglein, *Chem. Rev.*, 1989, **89**, 1861–1873.
89 M. Haruta, N. Yamada, T. Kobayashi and S. Iijima, *J. Catal.*, 1989, **115**, 301–309.
90 P. Gruene, D. M. Rayner, B. Redlich, A. F. G. van der Meer, J. T. Lyon, G. Meijer and A. Fielicke, *Science*, 2008, **321**, 674–676.
91 P. Chakraborty and T. Pradeep, *NPG Asia Mater.*, 2019, **11**, 48.
92 W. D. Knight, K. Clemenger, W. A. de Heer, W. A. Saunders, M. Y. Chou and M. L. Cohen, *Phys. Rev. Lett.*, 1984, **52**, 2141–2143.
93 R. E. Leuchtner, A. C. Harms and A. W. Castleman Jr., *J. Chem. Phys.*, 1989, **91**, 2753–2754.
94 D. E. Bergeron, A. W. Castleman, T. Morisato and S. N. Khanna, *Science*, 2004, **304**, 84–87.
95 S. N. Khanna and P. Jena, *Phys. Rev. B: Condens. Matter Mater. Phys.*, 1995, **51**, 13705–13716.
96 T. P. Martin, *Phys. Rep.*, 1996, **273**, 199–241.
97 S. Gilb, P. Weis, F. Furche, R. Ahlrichs and M. M. Kappes, *J. Chem. Phys.*, 2002, **116**, 4094–4101.
98 F. Furche, R. Ahlrichs, P. Weis, C. Jacob, S. Gilb, T. Bierweiler and M. M. Kappes, *J. Chem. Phys.*, 2002, **117**, 6982–6990.
99 A. Lechtken, C. Neiss, M. M. Kappes and D. Schooss, *Phys. Chem. Chem. Phys.*, 2009, **11**, 4344–4350.
100 B. Yoon, H. Häkkinen, U. Landman, A. S. Wörz, J.-M. Antonietti, S. Abbet, K. Judai and U. Heiz, *Science*, 2005, **307**, 403.
101 Z. Li, H. Y. T. Chen, K. Schouteden, T. Picot, T. W. Liao, A. Seliverstov, C. Van Haesendonck, G. Pacchioni, E. Janssens and P. Lievens, *Sci. Adv.*, 2020, **6**, eaay4289.
102 M. Brust, M. Walker, D. Bethell, D. J. Schiffrin and R. Whyman, *J. Chem. Soc., Chem. Commun.*, 1994, 801–802.
103 M. McPartlin, R. Mason and L. Malatesta, *J. Chem. Soc. D*, 1969, 334–334.
104 B. K. Teo, X. Shi and H. Zhang, *J. Am. Chem. Soc.*, 1992, **114**, 2743–2745.
105 G. Schmid, R. Pfeil, R. Boese, F. Bandermann, S. Meyer, G. H. M. Calis and J. W. A. van der Velden, *Chem. Ber.*, 1981, **114**, 3634–3642.
106 N. Jian, C. Stapelfeldt, K. J. Hu, M. Fröba and R. E. Palmer, *Nanoscale*, 2015, **7**, 885–888.
107 T. G. M. M. Kappen, P. P. J. Schlebos, J. J. Bour, W. P. Bosman, J. M. M. Smits, P. T. Beurskens and J. J. Steggerda, *Inorg. Chem.*, 1994, **33**, 754–758.
108 M. Bodiuzzaman and T. Pradeep, in *Atomically Precise Metal Nanoclusters*, ed. T. Pradeep, Elsevier, 2023, pp. 271–298.
109 R. L. Whetten, J. T. Khoury, M. M. Alvarez, S. Murthy, I. Vezmar, Z. L. Wang, P. W. Stephens, C. L. Cleveland, W. D. Luedtke and U. Landman, *Adv. Mater.*, 1996, **8**, 428–433.
110 Y. Shichibu, Y. Negishi, T. Tsukuda and T. Teranishi, *J. Am. Chem. Soc.*, 2005, **127**, 13464–13465.
111 D. Lee, R. L. Donkers, G. Wang, A. S. Harper and R. W. Murray, *J. Am. Chem. Soc.*, 2004, **126**, 6193–6199.
112 T. Carducci and R. Murray, in *Nanoelectrochemistry*, ed. S. A. Michael and V. Mirkin, CRC Press, Boca Raton, 2015, pp. 73–124.
113 Y. Negishi, K. Nobusada and T. Tsukuda, *J. Am. Chem. Soc.*, 2005, **127**, 5261–5270.
114 H. Häkkinen, M. Walter and H. Grönbeck, *J. Phys. Chem. B*, 2006, **110**, 9927–9931.
115 Y. Shichibu, Y. Negishi, T. Watanabe, N. K. Chaki, H. Kawaguchi and T. Tsukuda, *J. Phys. Chem. C*, 2007, **111**, 7845–7847.
116 S. C. K. Hau, P.-S. Cheng and T. C. W. Mak, *J. Am. Chem. Soc.*, 2012, **134**, 2922–2925.
117 Z. Wang, H. F. Su, X. P. Wang, Q. Q. Zhao, C. H. Tung, D. Sun and L. S. Zheng, *Chem. – Eur. J.*, 2018, **24**, 1640–1650.
118 Z. Wang, J. W. Liu, H. F. Su, Q. Q. Zhao, M. Kurmoo, X. P. Wang, C. H. Tung, D. Sun and L. S. Zheng, *J. Am. Chem. Soc.*, 2019, **141**, 17884–17890.
119 Z. Wang, Y. J. Zhu, Y. Z. Li, G. L. Zhuang, K. P. Song, Z. Y. Gao, J. M. Dou, M. Kurmoo, C. H. Tung and D. Sun, *Nat. Commun.*, 2022, **13**, 1802.
120 Z. G. Jiang, K. Shi, Y. M. Lin and Q. M. Wang, *Chem. Commun.*, 2014, **50**, 2353–2355.
121 S. Wang, Q. Li, X. Kang and M. Zhu, *Acc. Chem. Res.*, 2018, **51**, 2784.
122 K. M. Harkness, D. E. Cliffel and J. A. McLean, *Analyst*, 2010, **135**, 868–874.
123 T. Chen, Q. Yao, R. R. Nasaruddin and J. Xie, *Angew. Chem., Int. Ed.*, 2019, **58**, 11967–11977.
124 B. L. Nannenga and T. Gonen, *Emerging Top. Life Sci.*, 2018, **2**, 1–8.
125 S. Vergara, D. A. Lukes, M. W. Martynowycz, U. Santiago, G. Plascencia-Villa, S. C. Weiss, M. J. de la Cruz, D. M. Black, M. M. Alvarez, X. López-Lozano, C. O. Barnes, G. Lin, H. C. Weissker, R. L. Whetten, T. Gonen, M. J. Yacaman and G. Calero, *J. Phys. Chem. Lett.*, 2017, **8**, 5523–5530.
126 C. M. Aikens, *J. Phys. Chem. C*, 2008, **112**, 19797–19800.
127 J. Enkovaara, C. Rostgaard, J. J. Mortensen, J. Chen, M. Dułak, L. Ferrighi, J. Gavnholt, C. Glinsvad, V. Haikola, H. A. Hansen, H. H. Kristoffersen, M. Kuisma, A. H. Larsen, L. Lehtovaara, M. Ljungberg, O. Lopez-Acevedo, P. G. Moses, J. Ojanen, T. Olsen, V. Petzold, N. A. Romero, J. Stausholm-Møller, M. Strange, G. A. Tritsaris, M. Vanin, M. Walter, B. Hammer, H. Häkkinen, G. K. H. Madsen, R. M. Nieminen,

J. K. Nørskov, M. Puska, T. T. Rantala, J. Schiøtz, K. S. Thygesen and K. W. Jacobsen, *J. Phys.: Condens. Matter*, 2010, **22**, 253202.
128 K. L. D. M. Weerawardene and C. M. Aikens, *J. Am. Chem. Soc.*, 2016, **138**, 11202–11210.
129 P. Bose, G. Natarajan and T. Pradeep, *Atomically Precise Metal Nanoclusters*, Elsevier, 2023, pp. 313–343.
130 M. Walter, J. Akola, O. Lopez-Acevedo, P. D. Jadzinsky, G. Calero, C. J. Ackerson, R. L. Whetten, H. Grönbeck and H. Häkkinen, *Proc. Natl. Acad. Sci. U. S. A.*, 2008, **105**, 9157–9162.
131 P. D. Jadzinsky, G. Calero, C. J. Ackerson, D. A. Bushnell and R. D. Kornberg, *Science*, 2007, **318**, 430–433.
132 X. Kang, H. Chong and M. Zhu, *Nanoscale*, 2018, **10**, 10758–10834.
133 J. Akola, M. Walter, R. L. Whetten, H. Häkkinen and H. Grönbeck, *J. Am. Chem. Soc.*, 2008, **130**, 3756–3757.
134 M. W. Heaven, A. Dass, P. S. White, K. M. Holt and R. W. Murray, *J. Am. Chem. Soc.*, 2008, **130**, 3754–3755.
135 N. A. Sakthivel, S. Theivendran, V. Ganeshraj, A. G. Oliver and A. Dass, *J. Am. Chem. Soc.*, 2017, **139**, 15450–15459.
136 N. A. Sakthivel, M. Stener, L. Sementa, A. Fortunelli, G. Ramakrishna and A. Dass, *J. Phys. Chem. Lett.*, 2018, **9**, 1295–1300.
137 C. Kumara, X. Zuo, J. Ilavsky, D. Cullen and A. Dass, *J. Phys. Chem. C*, 2015, **119**, 11260–11266.
138 S. K. Eswaramoorthy, N. A. Sakthivel and A. Dass, *J. Phys. Chem. C*, 2019, **123**, 9634–9639.
139 H. Yang, Y. Wang, X. Chen, X. Zhao, L. Gu, H. Huang, J. Yan, C. Xu, G. Li and J. Wu, *Nat. Commun.*, 2016, **7**, 12809.
140 H. Qian, Y. Zhu and R. Jin, *Proc. Natl. Acad. Sci. U. S. A.*, 2012, **109**, 696.
141 C. Zeng, Y. Chen, K. Kirschbaum, K. J. Lambright and R. Jin, *Science*, 2016, **354**, 1580.
142 S. Vergara, U. Santiago, C. Kumara, D. Alducin, R. L. Whetten, M. J. Yacaman, A. Dass and A. Ponce, *J. Phys. Chem. C*, 2018, **122**, 26733–26738.
143 C. Kumara, M. M. Hoque, X. Zuo, D. A. Cullen, R. L. Whetten and A. Dass, *J. Phys. Chem. Lett.*, 2018, **9**, 6825–6832.
144 J. H. Beynon, *Microchim. Acta*, 1956, **44**, 437–453.
145 E. McDaniel, D. Martin and W. Barnes, *Rev. Sci. Instrum.*, 1962, **33**, 2–7.
146 F. W. McLafferty and T. A. Bryce, *Chem. Commun.*, 1967, 1215–1217.
147 A. Baksi, P. Chakraborty, A. Nag, D. Ghosh, S. Bhat and T. Pradeep, *Anal. Chem.*, 2018, **90**, 11351–11357.
148 Z. Luo, V. Nachammai, B. Zhang, N. Yan, D. T. Leong, D. E. Jiang and J. Xie, *J. Am. Chem. Soc.*, 2014, **136**, 10577–10580.
149 A. Baksi, P. Chakraborty, S. Bhat, G. Natarajan and T. Pradeep, *Chem. Commun.*, 2016, **52**, 8397–8400.
150 A. Baksi, A. Ghosh, S. K. Mudedla, P. Chakraborty, S. Bhat, B. Mondal, K. Krishnadas, V. Subramanian and T. Pradeep, *J. Phys. Chem. C*, 2017, **121**, 13421–13427.
151 P. Chakraborty, A. Baksi, S. K. Mudedla, A. Nag, G. Paramasivam, V. Subramanian and T. Pradeep, *Phys. Chem. Chem. Phys.*, 2018, **20**, 7593–7603.
152 P. Chakraborty, S. Malola, M. Neumaier, P. Weis, H. Häkkinen and M. M. Kappes, *Angew. Chem.*, 2023, e202305836.
153 P. Chakraborty, M. Neumaier, P. Weis and M. M. Kappes, *J. Am. Soc. Mass Spectrom.*, 2023, **34**, 676–684.
154 R. Yost and C. Enke, *J. Am. Chem. Soc.*, 1978, **100**, 2274–2275.
155 F. W. McLafferty, *Acc. Chem. Res.*, 1980, **13**, 33–39.
156 C. Zeng, T. Li, A. Das, N. L. Rosi and R. Jin, *J. Am. Chem. Soc.*, 2013, **135**, 10011–10013.
157 H. Qian, W. T. Eckenhoff, Y. Zhu, T. Pintauer and R. Jin, *J. Am. Chem. Soc.*, 2010, **132**, 8280–8281.
158 S. Malola, L. Lehtovaara, S. Knoppe, K.-J. Hu, R. E. Palmer, T. Bürgi and H. Häkkinen, *J. Am. Chem. Soc.*, 2012, **134**, 19560–19563.
159 C. Zeng, Y. Chen, C. Liu, K. Nobusada, N. L. Rosi and R. Jin, *Sci. Adv.*, 2015, **1**, e1500425.
160 C. Zeng, C. Liu, Y. Chen, N. L. Rosi and R. Jin, *J. Am. Chem. Soc.*, 2016, **138**, 8710–8713.
161 A. Dass, S. Theivendran, P. R. Nimmala, C. Kumara, V. R. Jupally, A. Fortunelli, L. Sementa, G. Barcaro, X. Zuo and B. C. Noll, *J. Am. Chem. Soc.*, 2015, **137**, 4610–4613.
162 A. Desireddy, B. E. Conn, J. Guo, B. Yoon, R. N. Barnett, B. M. Monahan, K. Kirschbaum, W. P. Griffith, R. L. Whetten and U. Landman, *Nature*, 2013, **501**, 399–402.
163 C. P. Joshi, M. S. Bootharaju, M. J. Alhilaly and O. M. Bakr, *J. Am. Chem. Soc.*, 2015, **137**, 11578–11581.
164 L. G. AbdulHalim, M. S. Bootharaju, Q. Tang, S. D. Gobbo, R. G. AbdulHalim, M. Eddaoudi, D. E. Jiang and O. M. Bakr, *J. Am. Chem. Soc.*, 2015, **137**, 11970–11975.
165 L. Cheng, Y. Yuan, X. Zhang and J. Yang, *Angew. Chem., Int. Ed.*, 2013, **52**, 9035–9039.
166 G. Natarajan, A. Mathew, Y. Negishi, R. L. Whetten and T. Pradeep, *J. Phys. Chem. C*, 2015, **119**, 27768–27785.
167 W. W. Xu, B. Zhu, X. C. Zeng and Y. Gao, *Nat. Commun.*, 2016, **7**, 13574.
168 H. Qian, Y. Zhu and R. Jin, *ACS Nano*, 2009, **3**, 3795–3803.
169 Y. Negishi, K. Munakata, W. Ohgake and K. Nobusada, *J. Phys. Chem. Lett.*, 2012, **3**, 2209–2214.
170 D. R. Kauffman, D. Alfonso, C. Matranga, H. Qian and R. Jin, *J. Phys. Chem. C*, 2013, **117**, 7914–7923.
171 K. Kwak, Q. Tang, M. Kim, D. Jiang and D. Lee, *J. Am. Chem. Soc.*, 2015, **137**, 10833–10840.
172 K. Kwak, V. D. Thanthirige, K. Pyo, D. Lee and G. Ramakrishna, *J. Phys. Chem. Lett.*, 2017, **8**, 4898.
173 K. Kwak and D. Lee, *Acc. Chem. Res.*, 2019, **52**, 12–22.
174 J. P. Wilcoxon, J. E. Martin, F. Parsapour, B. Wiedenman and D. F. Kelley, *J. Chem. Phys.*, 1998, **108**, 9137–9143.
175 Z. Wu and R. Jin, *ACS Nano*, 2009, **3**, 2036–2042.
176 H. Qian, M. Zhu, C. Gayathri, R. R. Gil and R. Jin, *ACS Nano*, 2011, **5**, 8935–8942.

177 T. G. Schaaff and R. L. Whetten, *J. Phys. Chem. B*, 2000, **104**, 2630–2641.
178 I. Dolamic, S. Knoppe, A. Dass and T. Bürgi, *Nat. Commun.*, 2012, **3**, 798.
179 S. Tian, Y. Z. Li, M. B. Li, J. Yuan, J. Yang, Z. Wu and R. Jin, *Nat. Commun.*, 2015, **6**, 8667.
180 I. Dolamic, B. Varnholt and T. Bürgi, *Phys. Chem. Chem. Phys.*, 2013, **15**, 19561–19565.
181 B. Varnholt, P. Oulevey, S. Luber, C. Kumara, A. Dass and T. Bürgi, *J. Phys. Chem. C*, 2014, **118**, 9604–9611.
182 E. Khatun, P. Chakraborty, B. R. Jacob, G. Paramasivam, M. Bodiuzzaman, W. A. Dar and T. Pradeep, *Chem. Mater.*, 2020, **32**, 611–619.
183 Y. Negishi, W. Kurashige and U. Kamimura, *Langmuir*, 2011, **27**, 12289–12292.
184 W. Kurashige, S. Yamazoe, K. Kanehira, T. Tsukuda and Y. Negishi, *J. Phys. Chem. Lett.*, 2013, **4**, 3181–3185.
185 Q. Xu, S. Wang, Z. Liu, G. Xu, X. Meng and M. Zhu, *Nanoscale*, 2013, **5**, 1176–1182.
186 I. Chakraborty, W. Kurashige, K. Kanehira, L. Gell, H. Häkkinen, Y. Negishi and T. Pradeep, *J. Phys. Chem. Lett.*, 2013, **4**, 3351–3355.
187 D. M. Chevrier, X. Meng, Q. Tang, D. Jiang, M. Zhu, A. Chatt and P. Zhang, *J. Phys. Chem. C*, 2014, **118**, 21730–21737.
188 P. Maity, S. Takano, S. Yamazoe, T. Wakabayashi and T. Tsukuda, *J. Am. Chem. Soc.*, 2013, **135**, 9450–9457.
189 Z. Lei, X. K. Wan, S. F. Yuan, J. Q. Wang and Q. M. Wang, *Dalton Trans.*, 2017, **46**, 3427–3434.
190 M. R. Narouz, K. M. Osten, P. J. Unsworth, R. W. Y. Man, K. Salorinne, S. Takano, R. Tomihara, S. Kaappa, S. Malola, C.-T. Dinh, J. D. Padmos, K. Ayoo, P. J. Garrett, M. Nambo, J. H. Horton, E. H. Sargent, H. Häkkinen, T. Tsukuda and C. M. Crudden, *Nat. Chem.*, 2019, **11**, 419–425.
191 C. M. Aikens, *Acc. Chem. Res.*, 2018, **51**, 3065–3073.
192 V. Linko, H. Zhang, Nonappa, M. A. Kostiainen and O. Ikkala, *Acc. Chem. Res.*, 2022, **55**, 1785–1795.
193 X. Kang, Y. Li, M. Zhu and R. Jin, *Chem. Soc. Rev.*, 2020, **49**, 6443–6514.
194 X. Kang and M. Zhu, *Chem. Soc. Rev.*, 2019, **48**, 2422–2457.
195 E. S. Shibu, M. A. H. Muhammed, T. Tsukuda and T. Pradeep, *J. Phys. Chem. C*, 2008, **112**, 12168–12176.
196 M. J. Hostetler, S. J. Green, J. J. Stokes and R. W. Murray, *J. Am. Chem. Soc.*, 1996, **118**, 4212.
197 Y. Song, T. Huang and R. W. Murray, *J. Am. Chem. Soc.*, 2003, **125**, 11694–11701.
198 R. Guo and R. W. Murray, *J. Am. Chem. Soc.*, 2005, **127**, 12140–12143.
199 J. F. Parker, J. E. F. Weaver, F. McCallum, C. A. Fields-Zinna and R. W. Murray, *Langmuir*, 2010, **26**, 13650–13654.
200 R. Guo, Y. Song, G. Wang and R. W. Murray, *J. Am. Chem. Soc.*, 2005, **127**, 2752–2757.
201 C. Zeng, C. Liu, Y. Pei and R. Jin, *ACS Nano*, 2013, **7**, 6138–6145.
202 A. Dass, A. Stevenson, G. R. Dubay, J. B. Tracy and R. W. Murray, *J. Am. Chem. Soc.*, 2008, **130**, 5940–5946.
203 A. C. Templeton, W. P. Wuelfing and R. W. Murray, *Acc. Chem. Res.*, 2000, **33**, 27–36.
204 C. L. Heinecke, T. W. Ni, S. Malola, V. Mäkinen, O. A. Wong, H. Häkkinen and C. J. Ackerson, *J. Am. Chem. Soc.*, 2012, **134**, 13316–13322.
205 T. W. Ni, M. A. Tofanelli, B. D. Phillips and C. J. Ackerson, *Inorg. Chem.*, 2014, **53**, 6500–6502.
206 L. G. Abdulhalim, N. Kothalawala, L. Sinatra, A. Dass and O. M. Bakr, *J. Am. Chem. Soc.*, 2014, **136**, 15865–15868.
207 Y. Chen, M. Zhou, Q. Li, H. Gronlund and R. Jin, *Chem. Sci.*, 2020, **11**, 8176–8183.
208 C. Zeng, H. Qian, T. Li, G. Li, N. L. Rosi, B. Yoon, R. N. Barnett, R. L. Whetten, U. Landman and R. Jin, *Angew. Chem., Int. Ed.*, 2012, **51**, 13114–13118.
209 C. Zeng, Y. Chen, A. Das and R. Jin, *J. Phys. Chem. Lett.*, 2015, **6**, 2976–2986.
210 L. C. McKenzie, T. O. Zaikova and J. E. Hutchison, *J. Am. Chem. Soc.*, 2014, **136**, 13426–13435.
211 S. Yang, S. Chen, L. Xiong, C. Liu, H. Yu, S. Wang, N. L. Rosi, Y. Pei and M. Zhu, *J. Am. Chem. Soc.*, 2018, **140**, 10988–10994.
212 A. Das, T. Li, G. Li, K. Nobusada, C. Zeng, N. L. Rosi and R. Jin, *Nanoscale*, 2014, **6**, 6458–6462.
213 M. S. Bootharaju, C. P. Joshi, M. J. Alhilaly and O. M. Bakr, *Chem. Mater.*, 2016, **28**, 3292–3297.
214 M. S. Bootharaju, V. M. Burlakov, T. M. D. Besong, C. P. Joshi, L. G. AbdulHalim, D. M. Black, R. L. Whetten, A. Goriely and O. M. Bakr, *Chem. Mater.*, 2015, **27**, 4289–4297.
215 E. Khatun, A. Ghosh, D. Ghosh, P. Chakraborty, A. Nag, B. Mondal, S. Chennu and T. Pradeep, *Nanoscale*, 2017, **9**, 8240–8248.
216 M. S. Bootharaju, R. Dey, L. E. Gevers, M. N. Hedhili, J.-M. Basset and O. M. Bakr, *J. Am. Chem. Soc.*, 2016, **138**, 13770–13773.
217 M. Bodiuzzaman, A. Ghosh, K. S. Sugi, A. Nag, E. Khatun, B. Varghese, G. Paramasivam, S. Antharjanam, G. Natarajan and T. Pradeep, *Angew. Chem., Int. Ed.*, 2019, **58**, 189–194.
218 C. K. Manju, D. Ghosh, M. Bodiuzzaman and T. Pradeep, *Dalton Trans.*, 2019, **48**, 8664–8670.
219 A. Jana, P. Chakraborty, W. A. Dar, S. Chandra, E. Khatun, M. P. Kannan, R. H. A. Ras and T. Pradeep, *Chem. Commun.*, 2020, **56**, 12550–12553.
220 X. Kang and M. Zhu, *Chem. Mater.*, 2019, **31**, 9939–9969.
221 Z. Wu and R. Jin, *Nano Lett.*, 2010, **10**, 2568–2573.
222 S. Wang, X. Zhu, T. Cao and M. Zhu, *Nanoscale*, 2014, **6**, 5777–5781.
223 A. Kim, C. Zeng, M. Zhou and R. Jin, *Part. Part. Syst. Charact.*, 2017, **34**, 1600388.
224 E. Khatun, A. Ghosh, P. Chakraborty, P. Singh, M. Bodiuzzaman, P. Ganesan, G. Nataranjan, J. Ghosh, S. K. Pal and T. Pradeep, *Nanoscale*, 2018, **10**, 20033–20042.

225 X. Kang, M. Zhou, S. Wang, S. Jin, G. Sun, M. Zhu and R. Jin, *Chem. Sci.*, 2017, **8**, 2581–2587.
226 E. Reyes, R. Madueño, M. Blázquez and T. Pineda, *J. Phys. Chem. C*, 2010, **114**, 15955–15962.
227 S. Knoppe, A. C. Dharmaratne, E. Schreiner, A. Dass and T. Bürgi, *J. Am. Chem. Soc.*, 2010, **132**, 16783–16789.
228 S. Knoppe, R. Azoulay, A. Dass and T. Bürgi, *J. Am. Chem. Soc.*, 2012, **134**, 20302–20305.
229 M. A. Habeeb Muhammed and T. Pradeep, *Chem. Phys. Lett.*, 2007, **449**, 186–190.
230 M. S. Bootharaju and T. Pradeep, *Langmuir*, 2011, **27**, 8134–8143.
231 W. Chen, X. Tu and X. Guo, *Chem. Commun.*, 2009, 1736–1738.
232 Z. Wu, *Angew. Chem., Int. Ed.*, 2012, **51**, 2934–2938.
233 J. Sun, H. Wu and Y. Jin, *Nanoscale*, 2014, **6**, 5449–5457.
234 M. S. Bootharaju, C. P. Joshi, M. R. Parida, O. F. Mohammed and O. M. Bakr, *Angew. Chem., Int. Ed.*, 2016, **55**, 922–926.
235 X. Kang, L. Xiong, S. Wang, H. Yu, S. Jin, Y. Song, T. Chen, L. Zheng, C. Pan, Y. Pei and M. Zhu, *Chem. – Eur. J.*, 2016, **22**, 17145–17150.
236 X. Kang, X. Wei, S. Jin, Q. Yuan, X. Luan, Y. Pei, S. Wang, M. Zhu and R. Jin, *Proc. Natl. Acad. Sci. U. S. A.*, 2019, **116**, 18834–18840.
237 M. S. Bootharaju, L. Sinatra and O. M. Bakr, *Nanoscale*, 2016, **8**, 17333–17339.
238 W. Du, S. Jin, L. Xiong, M. Chen, J. Zhang, X. Zou, Y. Pei, S. Wang and M. Zhu, *J. Am. Chem. Soc.*, 2017, **139**, 1618–1624.
239 W. J. Plieth, *Surf. Sci.*, 1985, **156**, 530–535.
240 R. A. Masitas and F. P. Zamborini, *J. Am. Chem. Soc.*, 2012, **134**, 5014–5017.
241 Z. Gan, N. Xia and Z. Wu, *Acc. Chem. Res.*, 2018, **51**, 2774–2783.
242 J. P. Choi, C. A. Fields-Zinna, R. L. Stiles, R. Balasubramanian, A. D. Douglas, M. C. Crowe and R. W. Murray, *J. Phys. Chem. C*, 2010, **114**, 15890–15896.
243 S. Tian, C. Yao, L. Liao, N. Xia and Z. Wu, *Chem. Commun.*, 2015, **51**, 11773–11776.
244 Z. Wu, M. Wang, J. Yang, X. Zheng, W. Cai, G. Meng, H. Qian, H. Wang and R. Jin, *Small*, 2012, **8**, 2028–2035.
245 C. Yao, J. Chen, M.-B. Li, L. Liu, J. Yang and Z. Wu, *Nano Lett.*, 2015, **15**, 1281–1287.
246 S. Wang, H. Abroshan, C. Liu, T.-Y. Luo, M. Zhu, H. J. Kim, N. L. Rosi and R. Jin, *Nat. Commun.*, 2017, **8**, 848.
247 X. Yuan, X. Dou, K. Zheng and J. Xie, *Part. Part. Syst. Charact.*, 2015, **32**, 613–629.
248 L. Liao, S. Zhou, Y. Dai, L. Liu, C. Yao, C. Fu, J. Yang and Z. Wu, *J. Am. Chem. Soc.*, 2015, **137**, 9511–9514.
249 Q. Li, S. Wang, K. Kirschbaum, K. J. Lambright, A. Das and R. Jin, *Chem. Commun.*, 2016, **52**, 5194–5197.
250 Q. Li, T. Y. Luo, M. G. Taylor, S. Wang, X. Zhu, Y. Song, G. Mpourmpakis, N. L. Rosi and R. Jin, *Sci. Adv.*, 2017, **3**, e1603193.
251 M. Zhu, P. Wang, N. Yan, X. Chai, L. He, Y. Zhao, N. Xia, C. Yao, J. Li, H. Deng, Y. Zhu, Y. Pei and Z. Wu, *Angew. Chem., Int. Ed.*, 2018, **57**, 4500–4504.
252 A. Das, T. Li, K. Nobusada, C. Zeng, N. L. Rosi and R. Jin, *J. Am. Chem. Soc.*, 2013, **135**, 18264–18267.
253 Y. Li, M. J. Cowan, M. Zhou, T.-Y. Luo, Y. Song, H. Wang, N. L. Rosi, G. Mpourmpakis and R. Jin, *J. Am. Chem. Soc.*, 2020, **142**, 20426–20433.
254 A. Fernando and C. M. Aikens, *J. Phys. Chem. C*, 2016, **120**, 14948.
255 Z. Wang, R. K. Gupta, F. Alkan, B.-L. Han, L. Feng, X.-Q. Huang, Z.-Y. Gao, C.-H. Tung and D. Sun, *J. Am. Chem. Soc.*, 2023, **145**, 19523–19532.
256 A. Sreekumaran Nair and T. Pradeep, *Curr. Sci.*, 2003, **84**, 1560–1564.
257 M. S. Bootharaju and T. Pradeep, *Langmuir*, 2012, **28**, 2671–2679.
258 M. S. Bootharaju, G. K. Deepesh, T. Udayabhaskararao and T. Pradeep, *J. Mater. Chem. A*, 2013, **1**, 611–620.
259 A. Mathew, G. Natarajan, L. Lehtovaara, H. Häkkinen, R. M. Kumar, V. Subramanian, A. Jaleel and T. Pradeep, *ACS Nano*, 2014, **8**, 139–152.
260 P. Chakraborty, A. Nag, G. Paramasivam, G. Natarajan and T. Pradeep, *ACS Nano*, 2018, **12**, 2415–2425.
261 P. Chakraborty, A. Nag, B. Mondal, E. Khatun, G. Paramasivam and T. Pradeep, *J. Phys. Chem. C*, 2020, **124**, 14891–14900.
262 P. Chakraborty, A. Nag, K. S. Sugi, T. Ahuja, B. Varghese and T. Pradeep, *ACS Mater. Lett.*, 2019, **1**, 534–540.
263 A. Nag, P. Chakraborty, G. Paramasivam, M. Bodiuzzaman, G. Natarajan and T. Pradeep, *J. Am. Chem. Soc.*, 2018, **140**, 13590–13593.
264 A. Nag, P. Chakraborty, A. Thacharon, G. Paramasivam, B. Mondal, M. Bodiuzzaman and T. Pradeep, *J. Phys. Chem. C*, 2020, **124**, 22298–22303.
265 M. A. H. Muhammed, L. K. Cruz, A. H. Emwas, A. M. El-Zohry, B. Moosa, O. F. Mohammed and N. M. Khashab, *Angew. Chem., Int. Ed.*, 2019, **58**, 15665–15670.
266 K. Sheng, Z. Wang, L. Li, Z. Y. Gao, C. H. Tung and D. Sun, *J. Am. Chem. Soc.*, 2023, **145**, 10595–10603.
267 S. Wang, Y. Song, S. Jin, X. Liu, J. Zhang, Y. Pei, X. Meng, M. Chen, P. Li and M. Zhu, *J. Am. Chem. Soc.*, 2015, **137**, 4018–4021.
268 K. R. Krishnadas, T. Udayabhaskararao, S. Choudhury, N. Goswami, S. K. Pal and T. Pradeep, *Eur. J. Inorg. Chem.*, 2014, **2014**, 908–916.
269 B. Zhang, G. Salassa and T. Bürgi, *Chem. Commun.*, 2016, **52**, 9205–9207.
270 B. Huang and Y. Pei, *J. Mater. Chem. A*, 2020, **8**, 10242–10251.
271 M. Neumaier, A. Baksi, P. Weis, E. K. Schneider, P. Chakraborty, H. Hahn, T. Pradeep and M. M. Kappes, *J. Am. Chem. Soc.*, 2021, **143**, 6969–6980.
272 P. Chakraborty, A. Nag, G. Natarajan, N. Bandyopadhyay, G. Paramasivam, M. K. Panwar, J. Chakrabarti and T. Pradeep, *Sci. Adv.*, 2019, **5**, eaau7555.

273 G. Salassa, A. Sels, F. Mancin and T. Bürgi, *ACS Nano*, 2017, **11**, 12609–12614.
274 A. Ghosh, T. Pradeep and J. Chakrabarti, *J. Phys. Chem. C*, 2014, **118**, 13959–13964.
275 A. Som, A. K. Samal, T. Udayabhaskararao, M. S. Bootharaju and T. Pradeep, *Chem. Mater.*, 2014, **26**, 3049–3056.
276 Nonappa and O. Ikkala, *Adv. Funct. Mater.*, 2018, **28**, 1704328.
277 Nonappa, *Chem. Commun.*, 2023, **59**, 13800–13819.
278 A. Som, I. Chakraborty, T. A. Maark, S. Bhat and T. Pradeep, *Adv. Mater.*, 2016, **28**, 2827–2833.
279 Nonappa, T. Lahtinen, J. S. Haataja, T. R. Tero, H. Häkkinen and O. Ikkala, *Angew. Chem., Int. Ed.*, 2016, **55**, 16035–16038.
280 A. Som, A. Griffo, I. Chakraborty, H. Hähl, B. Mondal, A. Chakraborty, K. Jacobs, P. Laaksonen, O. Ikkala, T. Pradeep and Nonappa, *Small*, 2022, **18**, 2201707.
281 A. Chakraborty, A. C. Fernandez, A. Som, B. Mondal, G. Natarajan, G. Paramasivam, T. Lahtinen, H. Häkkinen, Nonappa and T. Pradeep, *Angew. Chem., Int. Ed.*, 2018, **57**, 6522–6526.
282 A. Chakraborty, M. M. Stanley, B. Mondal, Nonappa, M. Bodiuzzaman, P. Chakraborty, M. P. Kannan and T. Pradeep, *Nanoscale*, 2023, **15**, 2690–2699.
283 J. Roy, B. Mondal, G. Vishwakarma, Nonappa, N. V. Sridharan, P. Krishnamurthi and T. Pradeep, *Nanoscale*, 2023, **15**, 8225–8234.
284 J. V. Rival, Nonappa and E. S. Shibu, *ACS Appl. Mater. Interfaces*, 2020, **12**, 14569–14577.
285 P. Bose, P. Chakraborty, J. S. Mohanty, Nonappa, A. Ray Chowdhuri, E. Khatun, T. Ahuja, A. Mahendranath and T. Pradeep, *Nanoscale*, 2020, **12**, 22116–22128.
286 A. Baksi, M. Gandi, S. Chaudhari, S. Bag, S. S. Gupta and T. Pradeep, *Angew. Chem., Int. Ed.*, 2016, **55**, 7777–7781.
287 A. Nag, A. Baksi, K. C. Krishnapriya, S. S. Gupta, B. Mondal, P. Chakraborty and T. Pradeep, *Eur. J. Inorg. Chem.*, 2017, **2017**, 3072–3079.
288 R. Kazan, U. Muller and T. Burgi, *Nanoscale*, 2019, **11**, 2938–2945.
289 P. Chakraborty, P. Bose, J. Roy, A. Nag, B. Mondal, A. Chakraborty and T. Pradeep, *J. Phys. Chem. C*, 2021, **125**, 16110–16117.
290 I. Chakraborty, T. Udayabhaskararao and T. Pradeep, *J. Hazard. Mater.*, 2012, **211–212**, 396–403.
291 H. Yang, Y. Wang, H. Huang, L. Gell, L. Lehtovaara, S. Malola, H. Häkkinen and N. Zheng, *Nat. Commun.*, 2013, **4**, 2422.
292 H. Qian, W. T. Eckenhoff, Y. Zhu, T. Pintauer and R. Jin, *J. Am. Chem. Soc.*, 2010, **132**, 8280–8281.